Supporting information

Unraveling Electro-Reductive Mechanisms of Biomass-Derived Aldehydes via Tailoring Interfacial Environments

Hengzhou Liu,[a] Deep M. Patel,[a] Yifu Chen,[a] Jungkuk Lee,[a] Ting-Han Lee,[a] Sarah D. Cady,[b] Eric W. Cochran,[a] Luke T. Roling,[*a] Wenzhen Li[*a]

a. Department of Chemical and Biological Engineering, Iowa State University, 618 Bissell Road, Ames, Iowa 50011, United States.

b. Department of Chemistry, Iowa State University, 2415 Osborn Drive, Ames, Iowa 50011, United States.

Corresponding authors:

Wenzhen Li − Department of Chemical and Biological Engineering, Iowa State University, 618 Bissell Road, Ames, Iowa 50011, United States; ORCID: 0000-0002-1020-5187; Email: wzli@iastate.edu

Luke T. Roling − Department of Chemical and Biological Engineering, Iowa State University, 618 Bissell Road, Ames, Iowa 50011, United States; ORCID:0000-0001-9742-2573; Email: roling@iastate.edu

Experimental section:

1. Chemicals and Materials

Potassium hydroxide (85%), furfural (99%), furfural alcohol (FA, 98%), 2-methylfuran (MF, 99%), 5-Methylfurfural (5-MF, 99%), 2,5-Dimethylfuran (DMF, 99%), 5-(hydroxymethyl)furfural (HMF, 99%), deuterium oxide (D_2O, 99.9 atom% D), sulfuric acid-d2 (96-98 wt. % in D_2O, 99.5 atom % D), HBF_4 (48 wt. % in H_2O), PbO (>99.9%, trace metal basis), and sodium sulfate (99%) were purchased from Sigma Aldrich. Acetonitrile (CH_3CN, HPLC grade), Dichloromethane (99.8%), lead foil (0.76 mm thick, 99.8%), platinum foil (0.025 mm thick, 99.9%), 2-propanol (99.9%), sulfuric acid (98%), potassium dibasic phosphate (≥98%), potassium monobasic phosphate (≥99%), potassium bicarbonate (99%), boric acid (≥99%), citric acid (99%), cetyltrimethylammonium bromide (CTAB, >99%), tetramethylammonium chloride (>99%), tetraethylammonium chloride (>99%), tetrapropylammonium chloride (>99%), tetrabutylammonium chloride (>99%), and tetrabutylammonium bromide (>99%) were purchased from Fisher Scientific. Acetonitrile-d3 (D, 99.8%) was purchased from Cambridge Isotopic Laboratories, InC. 5,5-Dimethyl-1-Pyrroline-N-Oxide (DMPO, 98%) was obtained from Matrix Scientific. H_2 calibration gases (10 ppm, 100 ppm, 1,000 ppm, 5,000 ppm, 10,000 ppm, balance helium) were purchased from Cal Gas Direct. Deionized (DI) water (18.2 MΩ cm, Barnstead™ E-Pure™) was used for all experiments in this work.

2. Preparation of Pb-based electrodes

OD-Pb was prepared in a standard three-electrode system in a one-compartment electrochemical cell by a modified method from literature.[1] A piece of Pb foil was sequentially polished by 380, 1200, and 2000 grit sandpaper and washed by DI-water and ethanol. Ag/AgCl (saturated KCl, Pine Research) and platinum foil served as the reference electrode and counter electrode, respectively. To synthesize OD-Pb-1, a symmetric square-wave pulse potential was applied on Pb foil from −1.00 to −0.40 $V_{Ag/AgCl}$ in a 0.2 M NaOH electrolyte at the frequency of 100 Hz for 2.5 h with both positive and negative scans. Subsequently, a constant potential (−1.3 $V_{Ag/AgCl}$) was applied for 10 min to obtain OD-Pb-1. To synthesize OD-Pb-2, the symmetric square-wave pulse potential was performed from −0.80 to −0.40 $V_{Ag/AgCl}$ in a 4.8 M H_2SO_4 electrolyte with the other procedures kept the same.

Electrodeposited Pb electrode was synthesized by a modification from previous literature.[2] A piece of polished Pb foil (2 cm^2) was immersed into 10 mM PbO with 1 M HBF_4 aqueous solution. Then, the electrodeposition was carried out in a standard three-electrode system by applying a constant current of −16 mA with 3.6 C total charge passed. The prepared electrodes were rinsed with deionized water and dried at room temperature.

To prepare drop-coated Pb, catalyst ink was prepared by dispersing lead powder in 2-propanol with added Nafion ionomer by ultrasonication. The mass ratio of Pb and Nafion ionomer was 4:1. The ink was then dropped onto the polished Pb foil to a final loading of ~2 $mg_{Pb}\,cm^{-2}$.

3. Materials Characterization

X-ray diffraction (XRD) crystallography was collected with a Siemens D500 diffractometer operated with a Cu Kα source (λ = 1.5418 Å) at 45 kV and 30 mA and equipped with a diffracted beam monochromator (carbon). Scanning Electron Microscopy-Energy Dispersive X-ray Spectroscopy (SEM-EDS) was conducted on a field-emission scanning electron microscope (FEI Quanta-250) equipped with a light-element X-ray detector and an Oxford Aztec energy-dispersive X-ray analysis system.

4. Electrochemical measurements in H-type cell on Pb foil

To perform electrochemical reduction in an H-type cell, a three-electrode configuration was set up with Ag/AgCl as the reference electrode and Pt foil as the counter electrode. The geometric area of the working

electrode was 2 cm^2. Anode and cathode compartments were separated by a Nafion membrane. The electrolyte was prepared with different concentration of sulfuric acid solutions or different pH of buffers, and 20 ml of the electrolyte was used in each compartment. Unless otherwise noted, CH_3CN/DI-water 1/3 (v/v) cosolvent was used in all experiments in order to fully dissolve the organic reactant. The resistance between the working and reference electrodes was determined by potentiostatic electrochemical impedance spectroscopy, and 90% *iR*-compensation was applied for all measurements.

Linear sweep voltammetry (LSV) and chronoamperometry (CA) tests were conducted under a constant Ar flow through the catholyte for deaeration and on-line analysis of evolved H_2 by gas chromatography (GC). LSV was carried out with a scan rate of 5 mV s^{-1} and without magnetic stirring. During CA tests, the catholyte and anolyte were stirred by PTFE-coated magnetic bars (20 × 6 mm, Chemglass Life Sciences) at 350 r.p.m. and the reaction time or the applied charge was controlled as constant (with details mentioned in the figure captions). The cathode chamber was connected to a sealed cold trap solution containing 25 ml CH_3CN, which was cooled to −10 ℃ by saltwater in order to absorb produced volatile MF or DMF. The on-line GC was connected in the reaction system to quantify generated H_2 from the cathode chamber, and the reactor configuration is shown in **Figure S1**. It should be noted that the products should be quantified immediately after each CA measurement to avoid any loss of MF or DMF. Potentials (*E*) were reported versus the reversible hydrogen electrode (RHE), as calculated by

$$E\ (\text{V vs. RHE}) = E\ (\text{V vs. Ag/AgCl}) + 0.197\ \text{V} + 0.059\ \text{V} \times \text{pH}$$

Conversion (X), product selectivity (S_i), and faradaic efficiency (FE_i) can be calculated by

$$X = \frac{n_0 - n}{n_0} \times 100\ \%$$

$$S_i = \frac{n_i}{n_0 - n} \times 100\ \%$$

$$FE_i = \frac{n_i z_i F}{Q} \times 100\ \%$$

Where n_0 is initial moles of reactant; n is the moles of reactant after electrolysis; n_i is the moles of product i; z_i is the number of electrons transferred for one product molecule; F is the Faraday constant (96,485 C mol^{-1}); Q is the total charge passed through the electrolytic cell.

Electrochemical impedance spectroscopy (EIS) measurements were taken at different applied potentials in furfural-containing solutions. The resulting Nyquist plots were fitted with an equivalent circuit of R1 + C2/R2 in the EC-Lab software, where R1 is the solution resistance, R2 is the charge transfer resistance, and C2 is the double layer capacitance. Surface roughness was determined from cyclic voltammetry in the potential range with charging/discharging current.

5. Electron Paramagnetic Resonance (EPR) measurements

Free radicals were generated by following the standard electrochemical tests. In order to generate sufficient free radicals with increased signal intensity of EPR, ECH of furfural was carried out in the phosphate-acetate buffer solution (pH = 5) at −0.79 V_{RHE}. During the CA test, 30 mg of DMPO was added to the electrolyte at 5 min of the reaction. After electrolysis of 1 hour, 1 ml of sample was immediately extracted and injected into a small quartz flat cell to perform EPR tests.

The EPR experiments were performed through a Bruker ELEXSYS E580 FT-EPR equipped with an ER 4122 SHQE resonator and a small quartz flat cell. Eight accumulated scans were acquired to measure DMPO-adducts until a steady-state spectrum with reduced noise was obtained. The detailed EPR settings are as follows: microwave frequency of 9.835 GHz, microwave power of 9.966 mW, center field of 3410 G, sweep width of 200 G, modulation amplitude of 1 G, receiver gain of 60 dB, time constant of 5.12 ms,

and sweep time of 20.97 s. The experimental EPR spectra were simulated and fitted by garlic (fast motion) function in EasySpin and MATLAB.[3]

6. Quantification method

6.1 High-Performance Liquid Chromatography (HPLC) for liquid products quantification

The electrolyte was analyzed by High-Performance Liquid Chromatography (HPLC, Agilent Technologies, 1260 Infinity II LC System) equipped with a variable wavelength detector (Agilent 1260 Infinity Variable Wavelength Detector VL). The wavelength of 210 and 225 nm was applied to quantify cathodic species from furfural and HMF reduction, respectively. Two isomers of the dimer product are reported together for simplicity. Detailed HPLC conditions were reported in our previous works.[4-5] In particular, the volatile products, MF from furfural reduction and 2,5-DMF from HMF reduction, were analyzed with the mobile phase of 1/1 (v/v) water/CH_3CN at a flow rate of 0.6 ml min^{-1} and detector wavelength of 210 nm.

6.2 On-line Gas chromatography (GC) for H_2 quantification

H_2 was quantified by on-line GC (SRI Instrument 8610C MG#3) equipped with HaySep D and MolSieve 5 Å columns and a thermal conductivity detector. The calibration curve was established by analyzing the standard calibration gases with different concentrations (10–10 000 ppm).

The GC program was started 2 min after the electrolysis was initiated, and a 6-min programmed cycle (including a 4-min running period and a 2-min cooling period) was repeated throughout the measurement.

The rate of H_2 generation (r, mol s^{-1}) for each cycle was calculated by:

$$r = c \times 10^{-6} \times [p\dot{V} \times 10^{-6}/(RT)]$$

Where c is the H_2 concentration (ppm); $\dot{V}$ is the volumetric flow rate of the inlet gas (12.5 mL min^{-1}); p is the ambient pressure (p = 1.013 × 10^5 Pa); R is the gas constant (R = 8.314 J mol^{-1} K^{-1}); T is the room temperature (293.15 K). The total amount of H_2 production (mol) was calculated by integrating the plot of H_2 production rate (mol s^{-1}) *vs.* reaction time (s) with polynomial curve fitting.

6.3 Gas chromatography-mass spectrometry (GC-MS) for isotopic incorporation study

Aqueous products were analyzed by gas chromatography (GC, Agilent 7890B) connected with a mass spectrometry (MS, Agilent 5977A). GC was equipped with a flame ionization detector (FID) detector and a capillary column (0.18 mm ID, 1.63 m × 180 μm × 0 μm). The temperature program of GC was initiated at 40 ℃, held for 5 min, and ramped to 200 ℃ with a rate of 15 ℃ min^{-1}. The volume of injected sample was 0.5 μL. Helium (99.999%) with a flow rate of 1.0 ml min^{-2} was used as the carrier gas. Samples from the catholyte were diluted, NaCl-saturated, and extracted by dichloromethane. The organic layer was collected and filtered by 0.22 μm filters for analysis. The purpose of adding NaCl was to increase the efficiency of phase separation between two immiscible solvents. The MF-containing trapping solution (MF in CH_3CN) was directly filtered and injected to GC-MS for analysis. All mass fragments with the m/z values in the range of 10 to 110 were scanned and recorded. To identify the product, the acquired MS results were compared with NIST database. It should be noted that the samples after electrolysis should be immediately prepared for its analysis in GC-MS to avoid H-D exchange and evaporation.

6.4 NMR for identification of the isotopic product

Reaction aliquots were sampled and analyzed by ^1H NMR spectroscopy. ^1H NMR was performed by a Bruker 600 MHz NMR spectrometer (AVIII-600). After electrolysis, NaCl-saturated catholyte was first extracted by dichloromethane solution, and the organic layer was collected in a separate vial. Then the dichloromethane solvent (boiling point of 39.6°C) was evaporated by feeding Ar gas, and the small amounts

of non-volatile furfural- and FA-containing solutions remaining in the vial was re-dissolved in acetonitrile-d3 solvent for NMR analysis (a scheme of these procedures was shown in **Figure S5**). Volatile product MF trapped in 3 ml of acetonitrile-d3 cold solvent was directly collected for NMR analysis. The amount of deuterium was determined by comparing proton signal of the hydroxyl group, or the proton signal at α-carbon of the hydroxyl, to the proton signals of the furan ring. In addition, standard compounds (MF, FA, and furfural) dissolved in acetonitrile-d3 solvent were also analyzed by NMR for product identification and comparison.

7. Quantification of O_2 concentration in the electrolyte.

The concentration of dissolved O_2 in the electrolyte was measured by Winkler method through an iodine-thiosulfate redox titration.[6] 50 ml of electrolyte [0.5 M H_2SO_4 in 1/3 (v/v) CH_3CN/DI-water cosolvent] was first saturated by purging O_2, followed by adding 0.5 mL of 3 M $MnSO_4$ and 1 ml of solution with 4 M KOH and 2 M KI under vigorous stirring to react with all dissolved O_2 into a brown precipitation. Then, 1 ml of 5 M H_2SO_4 was added to fully acidify the solution, and iodide (I^-) was oxidized to free iodine (I_2) by MnO_2. Finally, the I_2-containing solution was titrated by a NaS_2O_3 solution with a known concentration. A starch indicator was used to monitor the color change. The amount of O_2 in the solution can be calculated by the molar ratio of O_2: $Na_2S_2O_3$ is 4:1. The reactions sequentially occurred in this process are shown as follows:

$$2Mn^{2+}_{(aq)} + O_{2(aq)} + 4OH^-_{(aq)} \rightarrow 2MnO(OH)_{2(s)}$$

$$MnO(OH)_{2(s)} + 4H^+_{(aq)} + 2I_{(aq)} \rightarrow Mn^{2+}_{(aq)} + I_{2(aq)} + 3H_2O_{(l)}$$

$$I_{2(aq)} + 2S_2O_3{}^{2-}_{(aq)} \rightarrow 2I^-_{(aq)} + S_4O_6{}^{2-}_{(aq)}$$

8. Computational details

Plane wave density functional theory calculations were performed using the Vienna ab initio Simulation Package (VASP).[7-10] Project augmented-wave (PAW) potentials were used to quantify electron-ion interactions. The generalized gradient approximation (GGA)[11-12] and Perdew-Burke-Ernzerhof (PBE) functional were used to calculate exchange correlations.[13] Dispersion corrections were included using the DFT-D3 method.[14-15] Dipole corrections[16] were implemented along the z-direction (i.e., perpendicular to the modeled crystalline (111) slab). Ionic forces were converged to 0.02 eV/Å, and the tolerance of electronic energies was set to 10^{-4} eV. The kinetic energy cutoff was set to 400 eV. All thermodynamic Gibbs free energies were referenced to the clean surface and gas phase free energies of furfural (F) and hydrogen (H_2). For a given species A* on the surface, its free energy (G_{A*}) is therefore calculated as:

$$G_{A*} = (E_A + ZPE_A - TS_A) - E_{surf} - n\left(E_{F,g} + ZPE_{F,g} - TS_{F,g}\right) - m\left(E_{H_2,g} + ZPE_{H_2,g} - TS_{H_2,g}\right)$$

Here, E_i is the DFT-calculated energy of the optimized structure of species i, ZPE_i is the calculated zero-point energy of species i, and S_i is the calculated entropy of species i. ZPE and S were calculated according to a harmonic oscillator approximation. The temperature (T) is 298.15 K in accordance with experimental conditions. The constants m and n are coefficients for stoichiometric balance.

The free energies of elementary electrochemical steps are corrected by adding |e|*U (where U is the electrode potential vs. RHE) term to the reaction energies according to Nørskov's computational hydrogen electrode (CHE) model.[17] Transition states and activation energies for surface-mediated elementary steps were calculated using the climbing image nudged elastic band theory.[18-19] An additional linear correction term $\beta*(U-U_0)$ is applied as proposed by Janik and coworkers to account for electrode potential; U_0 is the onset potential for coadsorption of H* (referenced to $H_{2(g)}$) on a given surface in the presence of the other reactant molecule for the hydrogenation step.[20] We assume the value of symmetry factor (β) to be 0.5, acknowledging potential limitations of this assumption.[21]

We note that quantifying the relative flux through Langmuir Hinshelwood (LH)-type mechanisms and Eley Rideal (ER)-type mechanisms is complicated due to the difficulty of quantifying coverage effects and potential effects in reaction energetics. This also inhibits our ability to comment directly on the dependence of reaction mechanisms on applied potential, as the reaction fluxes are determined by more than just reaction energetics calculated on clean surfaces.

A 4 x 4 x 4 periodic unit cell of Pb(111) was used for all surface calculations. The bottom two layers were fixed at their bulk positions, and other atoms were allowed to relax. A 4 x 4 x 1 gamma-centered Monkhorst-Pack k-point grid [22] was used for sampling in the Fourier space. Approximately 12 atomic layers of vacuum spacing was provided in the z-direction to avoid any spurious interactions between periodic images of system in that dimension. The lattice constant of Pb was calculated to be 4.97 Å, which is in good agreement with experimental value of 4.93 Å.[23]

Solution phase Gibbs free energy of reactions and activation energies were calculated with Gaussian 09[24] using the B3LYP functional and the 6-311++G(d,p) basis set.[25-26] The presence of water (solvent) was modeled using the SMD variant of Polarizable Continuum Model (PCM) with the integral equation formalism variant.[27]

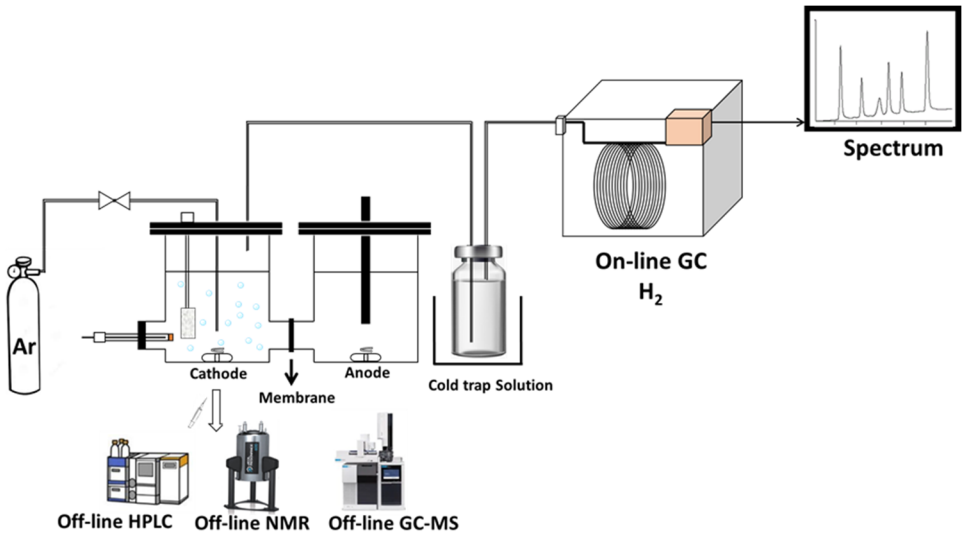

Figure S1. The experimental setup for ECH of furfural, including the H-type cell, cold trapping solution, on-line GC for H_2 quantification, and off-line identification/quantification of FA, MF, and hydrofuroin by HPLC, NMR, or GC-MS.

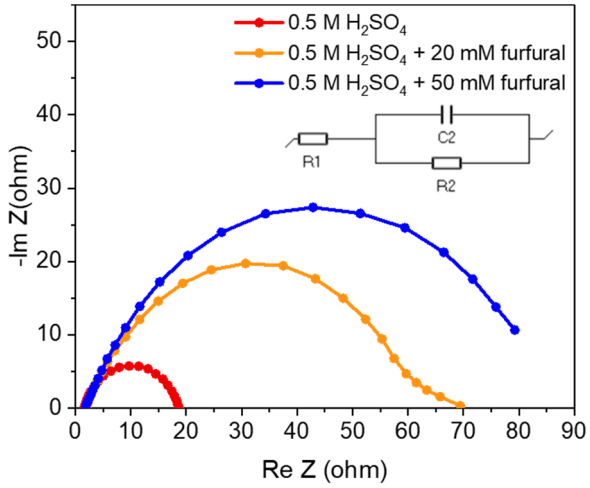

Figure S2. Nyquist plots on Pb foil in four different solutions: 0.5 M H_2SO_4 (red curve), 0.5 M H_2SO_4 + 20 mM furfural (yellow curve), 0.5 M H_2SO_4 + 50 mM furfural (blue curve). All electrolytes were prepared in 1:3 (v/v) CH_3CN/H_2O co-solvent. Inset showed the equivalent circuit of the double layer.

The diameter of semi-circles in the Nyquist plot increased with the addition of furfural, suggesting a suppressed electron transfer. This result supported the competitive adsorption of furfural and H on Pb surface, because the diameter of the semi-circles was related to the charge transfer resistance of the Volmer step for H adsorption, with the increased diameters corresponding to a sluggish kinetics.[28] In the aqueous phase, to adsorb these organic molecules on the electrode surface, the adjacent solvent environment is displaced, and meanwhile the local chemical environment and charge transfer dynamics are altered accordingly.[29-31] Similar competing adsorptions were observed in the electroreduction of other aldehyde compounds (e.g., benzaldehyde and phenol,[32-34] cyclohexanecarboxaldehyde and heptanal[35]).

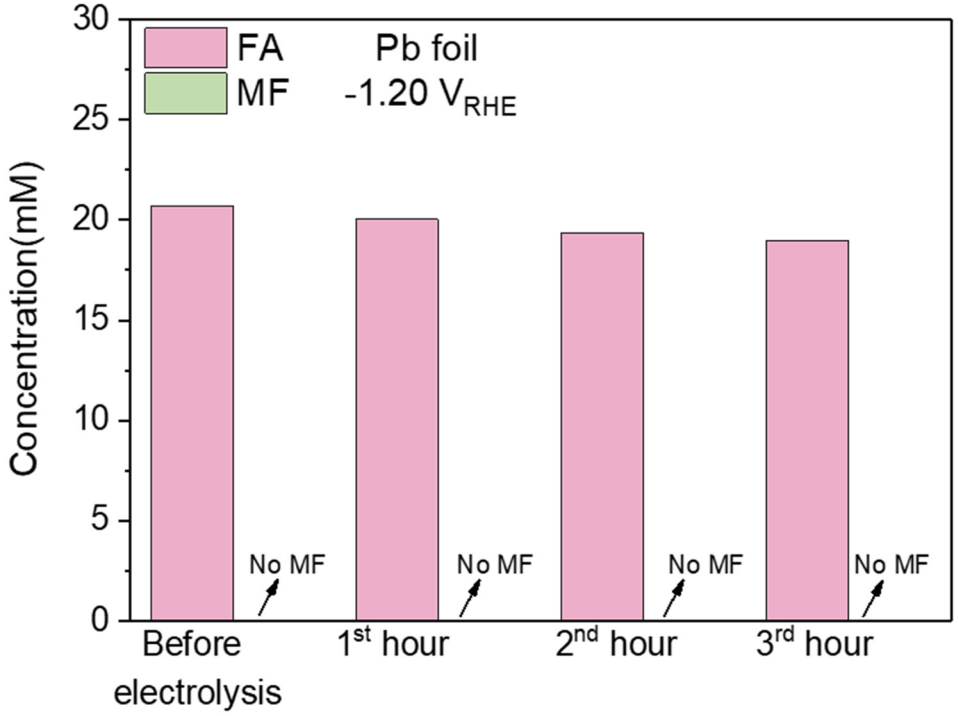

Figure S3. Electrolysis of FA on Pb electrode. The concentration of reactant FA and product MF for 3-hour electrolysis on Pb foil at −1.20 V_{RHE}. The electrolyte was 20 mM furfural in 1:3 (v/v) CH_3CN/H_2O co-solvent with 0.5 M H_2SO_4. The electrolyte was analyzed at each 1-hour interval. The slight decrease in FA concentration could be due to its slight degradation in strong acid conditions.

Supporting information, note 1 (Figure S4-S13 and Table S1-S5): Isotopic product analysis by Gas chromatography–mass spectrometry (GC-MS) and ^{1}H-NMR

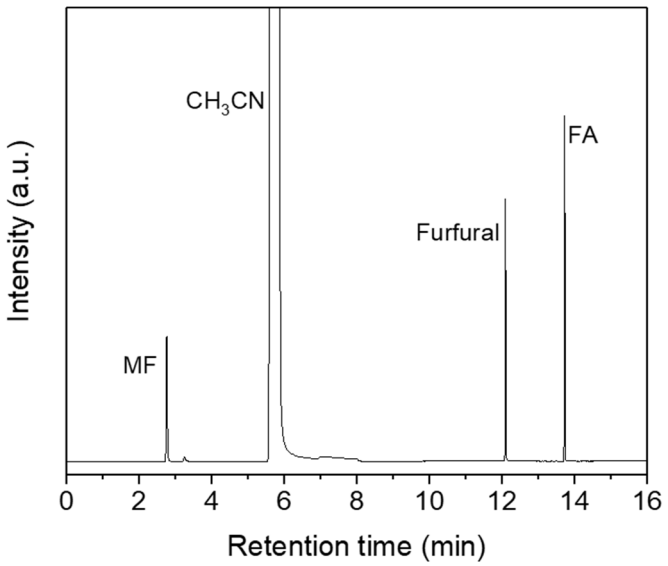

Figure S4. The typical GC chromatogram for standard furfural, FA, and MF in the CH_3CN solvent.

Table S1. GC-MS result of the sample after 1-hour electrolysis at −1.20 V_{RHE}. The electrolyte is 20 mM furfural and 0.5 M **H_2SO_4** in 1:3 (v/v) **CH_3CN/H_2O** co-solvent.[a]

Reaction Condition	Fragment of FA (m/z)	Abundance (a.u.)	Percentage (%)	Fragment of MF (m/z)	Abundance (a.u.)	Percentage (%)
	95	1946	5.96	81	29113	37.04
20 mM furfural	96	798	2.44	82	46383	59.02
0.5 M **H_2SO_4**	97	9875	30.25	83	2834	3.61
1:3 (v/v)	98	18939	58.02	84	259	0.33
CH_3CN/H_2O	99	1065	3.26	85	0	0
	100	18	0.06	86	0	0
Total		32640	100		78589	100

a. The MS result in this table is compared with the standard FA and MF in the CH_3CN solvent and agreed well with the database from NIST chemistry webbook.

Table S2. GC-MS result of the sample after 1-hour electrolysis at −1.20 V_{RHE}. The electrolyte is 20 mM furfural and 0.5 M **D_2SO_4** in 1:3 (v/v) **CH_3CN/H_2O** co-solvent.

Reaction Condition	Fragment of FA (m/z)	Abundance (a.u.)	Percentage (%)	Fragment of MF (m/z)	Abundance (a.u.)	Percentage (%)
20 mM furfural 0.5 M **D_2SO_4** 1:3 (v/v) **CH_3CN/H_2O**	95	1826	5.07	81	9347	36.79
	96	806	2.24	82	14624	57.56
	97	10768	29.91	83	1100	4.33
	98	21536	59.83	84	336	1.32
	99	1061	2.95	85	0	0
	100	0	0	86	0	0
Total		35997	100		25407	100

Table S3. GC-MS result of the sample after 1-hour electrolysis at −1.20 V_{RHE}. The electrolyte is 20 mM furfural and 0.5 M **D_2SO_4** in 1:3 (v/v) **CH_3CN/D_2O** co-solvent.

Reaction Condition	Fragment of FA (m/z)	Abundance (a.u.)	Percentage (%)	Fragment of MF (m/z)	Abundance (a.u.)	Percentage (%)
20 mM furfural 0.5 M **D_2SO_4** 1:3 (v/v) **CH_3CN/D_2O**	95	2246	4.43	81	335	0.27
	96	392	0.77	82	17181	13.62
	97	3561	7.02	83	24690	19.57
	98	12115	23.90	84	70493	55.88
	99	30312	59.80	85	12722	10.08
	100	2067	4.08	86	739	0.59
Total		50693	100		126159	100

Table S4. GC-MS result of the sample after 1-hour electrolysis at −1.20 V_{RHE}. The electrolyte is 20 mM furfural and 0.5 M **H_2SO_4** in 1:3 (v/v) **CH_3CN/D_2O** co-solvent.

Reaction Condition	Fragment of FA (m/z)	Abundance (a.u.)	Percentage (%)	Fragment of MF (m/z)	Abundance (a.u.)	Percentage (%)
20 mM furfural 0.5 M **H_2SO_4** 1:3 (v/v) **CH_3CN/D_2O**	95	1201	5.16	81	0	0
	96	251	1.08	82	5965	14.24
	97	1802	7.74	83	8735	20.85
	98	5561	23.90	84	22920	54.72
	99	13392	57.55	85	4046	9.66
	100	1062	4.56	86	223	0.53
Total		23269	100		41889	100

Table S5. GC-MS result of the sample after 1-hour electrolysis at −1.20 V_{RHE}. The electrolyte is 20 mM furfural and 0.5 M **H_2SO_4** in 1:3 (v/v) **CD_3CN/H_2O** co-solvent.

Reaction Condition	Fragment of FA (m/z)	Abundance (a.u.)	Percentage (%)	Fragment of MF (m/z)	Abundance (a.u.)	Percentage (%)
20 mM furfural 0.5 M **H_2SO_4** 1:3 (v/v) **CD_3CN/H_2O**	95	1597	4.99	81	9379	37.08
	96	731	2.28	82	14933	59.04
	97	9513	29.73	83	980	3.87
	98	19064	59.57	84	0	0
	99	942	2.94	85	0	0
	100	155	0.48	86	0	0
Total		32002	100		25292	100

Note: Table S1-S5 suggested that the proton source for FA and MF is from H_2O, not CH_3CN. Although the absolute abundance of each m/z ratio varies, their percentage values are similar and only depends on the electrolyte compositions that can provide protons. It should be noted that it is hard to experimentally track the proton source from acid or water. This is because ionized proton in H_2SO_4 would be quickly exchanged with H_2O and attain an equilibrium. For instance, for the isotopic experiments with 0.5 M D_2SO_4 (1 M of D) in 1:3 (v/v) CH_3CN/H_2O co-solvent (83.3 M of H in H_2O, as CH_3CN cannot provide H source), because of their quick equilibrium after adding D_2SO_4 in co-solvent, the acid H and water H would be equal and cannot be differentiated. That is, for acid, it contains 83.3/84.3 of H_2SO_4 + 1/84.3 of D_2SO_4. The same ratio in water: 83.3/84.3 of H_2O + 1/84.3 of D_2O. In general, there would have a fast equilibrium between DH_2O^+, H_3O^+ (the majority protonated species), HDO, H_2O (still the majority overall species), etc. as the H/D are transferred quickly among the water molecules.

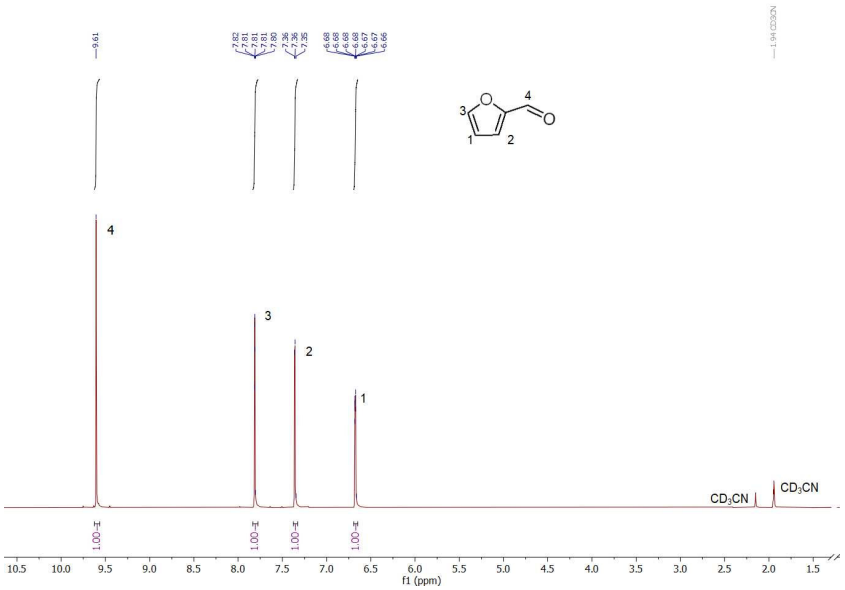

Figure S5. **^{1}H NMR result of standard furfural in CD_3CN solvent**. ^{1}H NMR (600 MHz, CD_3CN) δ 9.61 (s, 1H), 7.83 – 7.78 (m, 1H), 7.36 (d, *J* = 3.6 Hz, 1H), 6.68 (dt, *J* = 3.5, 1.2 Hz, 1H). The peak area ratio in the position 1, 2, 3, and 4 are 1.00:1.00:1.00:1.00, respectively.

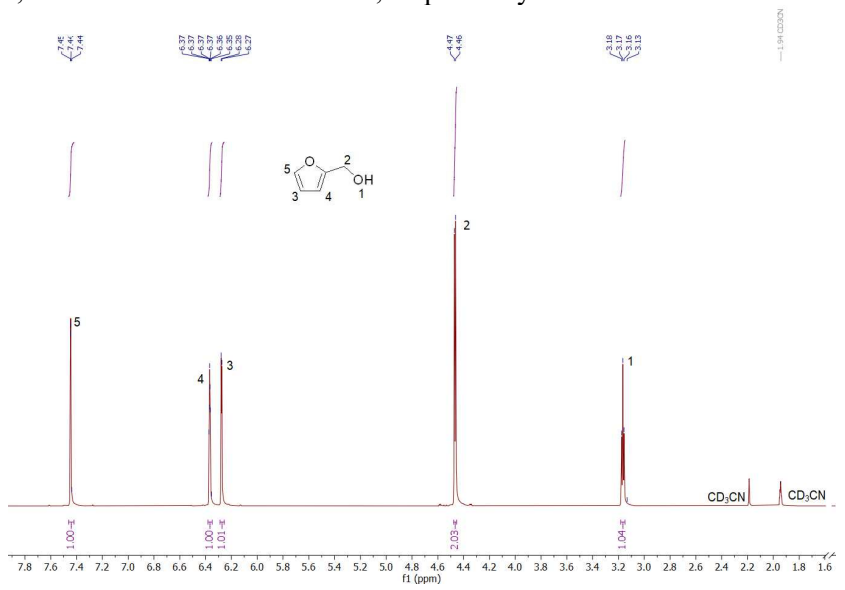

Figure S6. **^{1}H NMR result of standard furfuryl alcohol in CD_3CN solvent**. ^{1}H NMR (600 MHz, CD_3CN) δ 7.45 (d, *J* = 1.8 Hz, 1H), 6.37 (dt, *J* = 3.0, 1.2 Hz, 1H), 6.28 (d, *J* = 3.3 Hz, 1H), 4.47 (d, *J* = 5.7 Hz, 2H), 3.17 (t, *J* = 5.9 Hz, 1H). The peak area ratio in the position 1, 2, 3, 4 and 5 are 1.04:2.03:1.00:1.00:1.00, respectively.

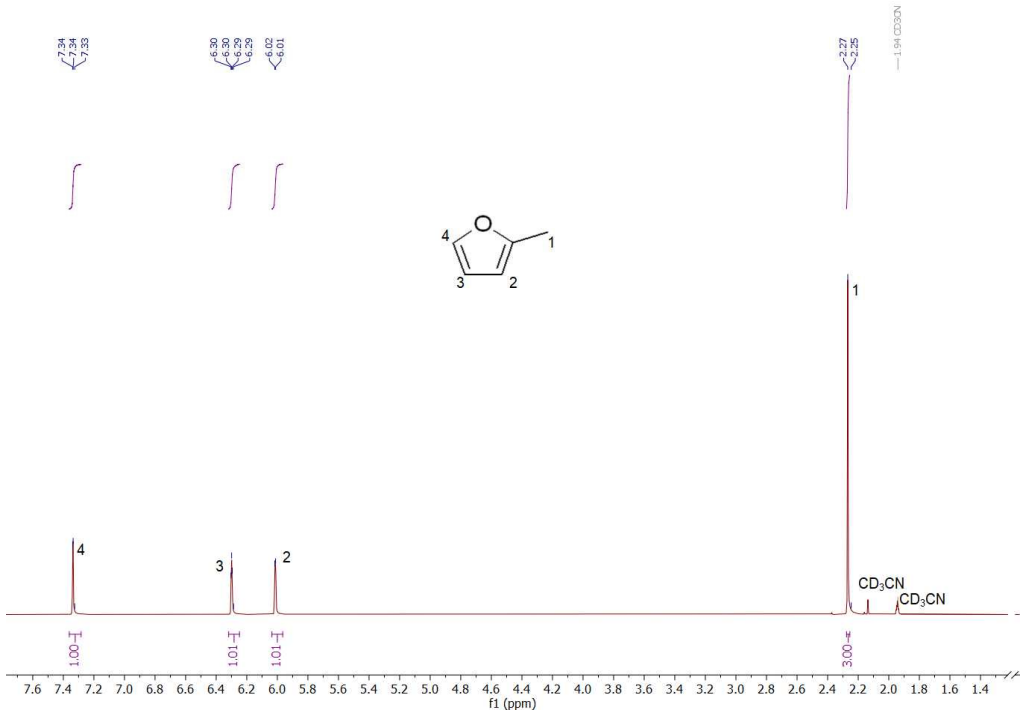

Figure S7. ^{1}H NMR result of standard 2-Methylfuran in CD_3CN solvent. ^{1}H NMR (600 MHz, CD_3CN) δ 7.34 (d, *J* = 1.9 Hz, 1H), 6.30 (t, *J* = 2.6 Hz, 1H), 6.01 (d, *J* = 3.1 Hz, 1H), 2.27 (s, 3H). The peak area ratio in the position 1, 2, 3 and 4 are 3.00:1.01:1.01:1.00, respectively.

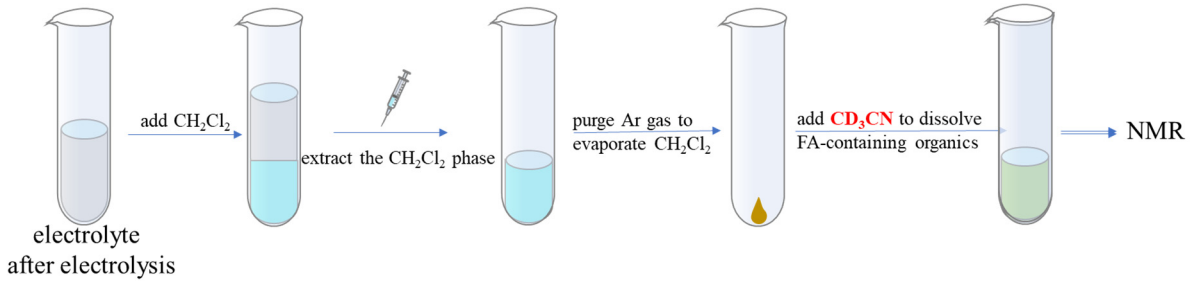

Figure S8. **The procedure of the measurement of FA-containing sample after electrolysis by NMR**. The sample after electrolysis was extracted by CH_2Cl_2, followed by the evaporation of CH_2Cl_2 solvent through purging Ar gas at room temperature, and the remaining organic phase with FA-containing solutions was re-dissolved in CD_3CN solvent and tested by NMR.

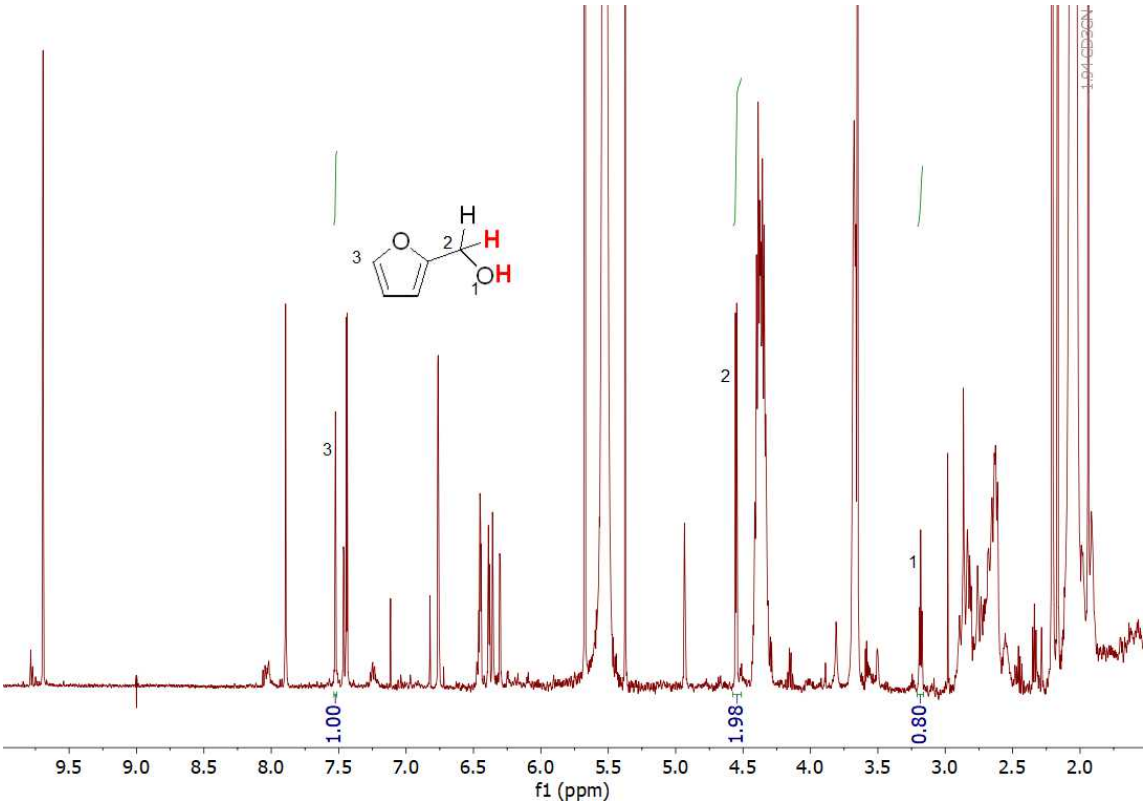

Figure S9. ^{1}H NMR test result of the sample after electrolysis in H-only electrolyte. H-only electrolyte was prepared by dissoving 20 mM furfural in the electrolyte with 0.5 M H_2SO_4 in 1:3 (v/v) CH_3CN/H_2O co-solvent. The 1-hour electrolysis was performed on Pb foil at −1.20 V_{RHE}. After the electrolysis, the FA-containing sample was prepared by the sequence as shown in **Figure S8**. The ratios in peak area in the position 1, 2, and 3 are 0.80:1.98:1.00, respectively, which almost agreed with the standard sample of FA in **Figure S6**.

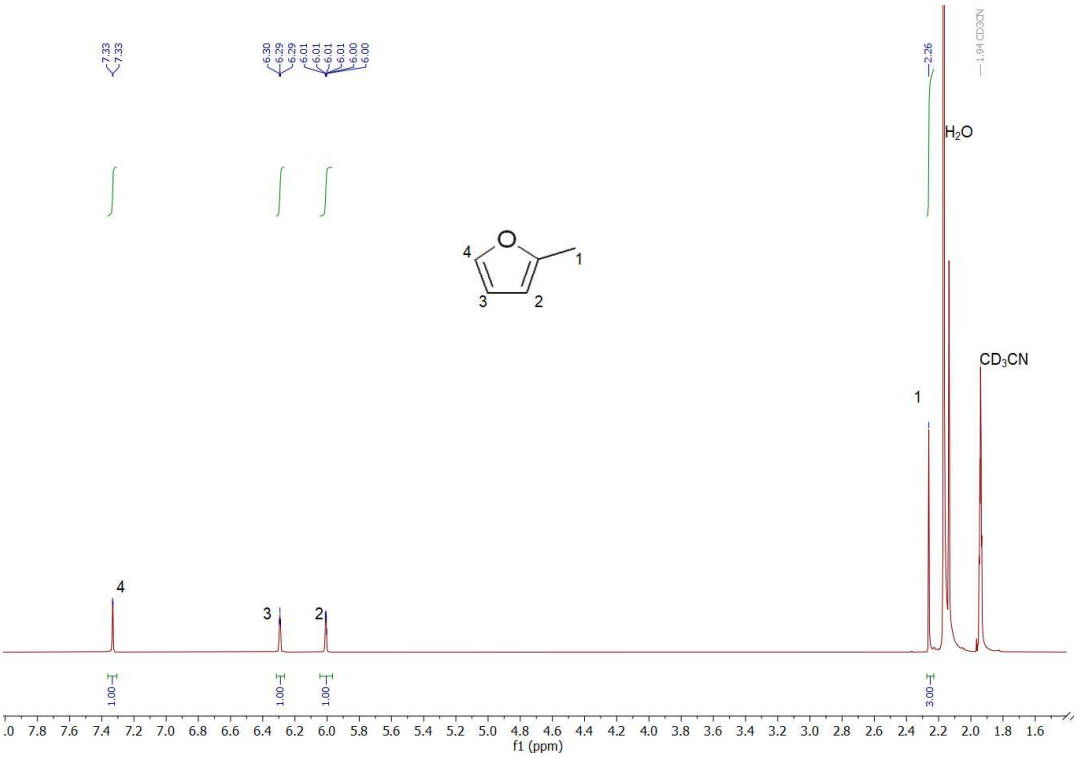

Figure S10. ^{1}H NMR test result of the trapping solution after electrolysis in H-only electrolyte. H-only electrolyte was prepared by dissoving 20 mM furfural in the electrolyte with 0.5 M H_2SO_4 in 1:3 (v/v) CH_3CN/H_2O co-solvent. The 1-hour electrolysis was performed on Pb foil at −1.20 V_{RHE}. The solution in trapping of volatile MF was CD_3CN solvent in ice-water bath (**Figure S1**). The peak area ratios in the position 1, 2, 3, and 4 are 3.00:1.00:1.00:1.00, respectively, which agreed well with the standard sample of MF in **Figure S8**.

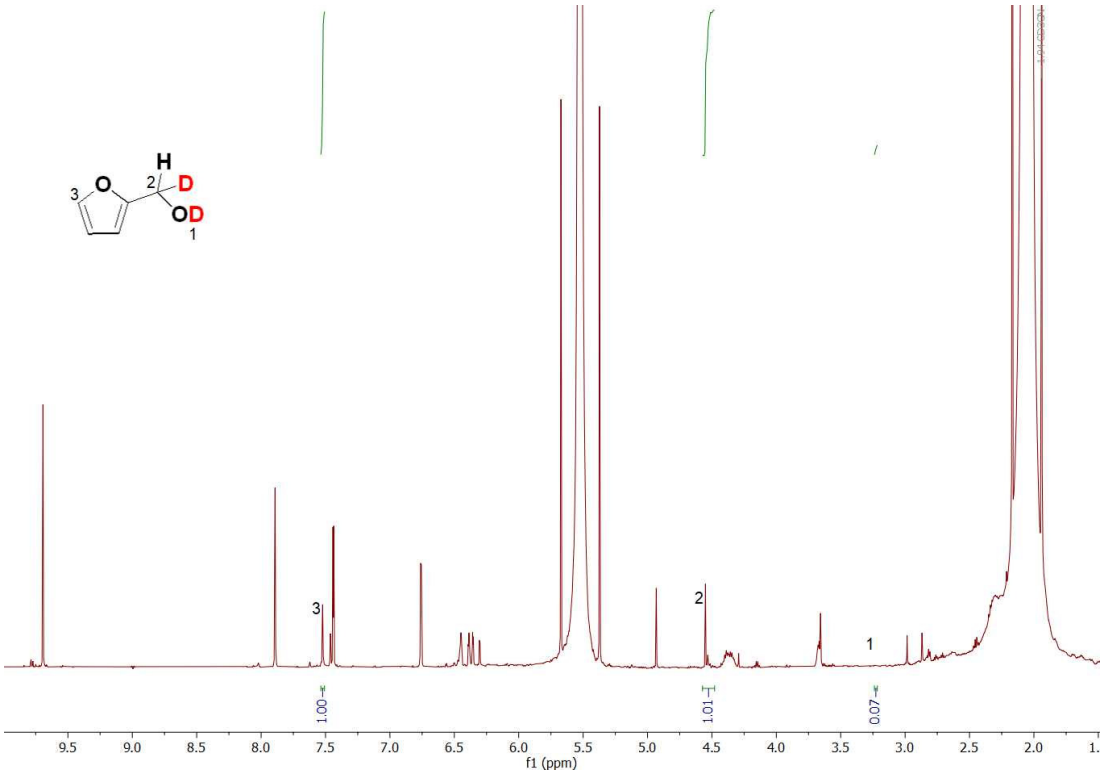

Figure S11. ^{1}H NMR test result of the sample after electrolysis in D-only electrolyte. D-only electrolyte was prepared by dissoving 20 mM furfural in the electrolyte with 0.5 M D_2SO_4 in 1:3 (v/v) CD_3CN/D_2O co-solvent. The 1-hour electrolysis was performed on Pb foil at −1.20 V_{RHE}. After the electrolysis, the FA-containing sample was prepared by the sequence as shown in **Figure S8**. The peak area ratios in the position 1, 2, and 3 are 0.07:1.01:1.00, respectively.

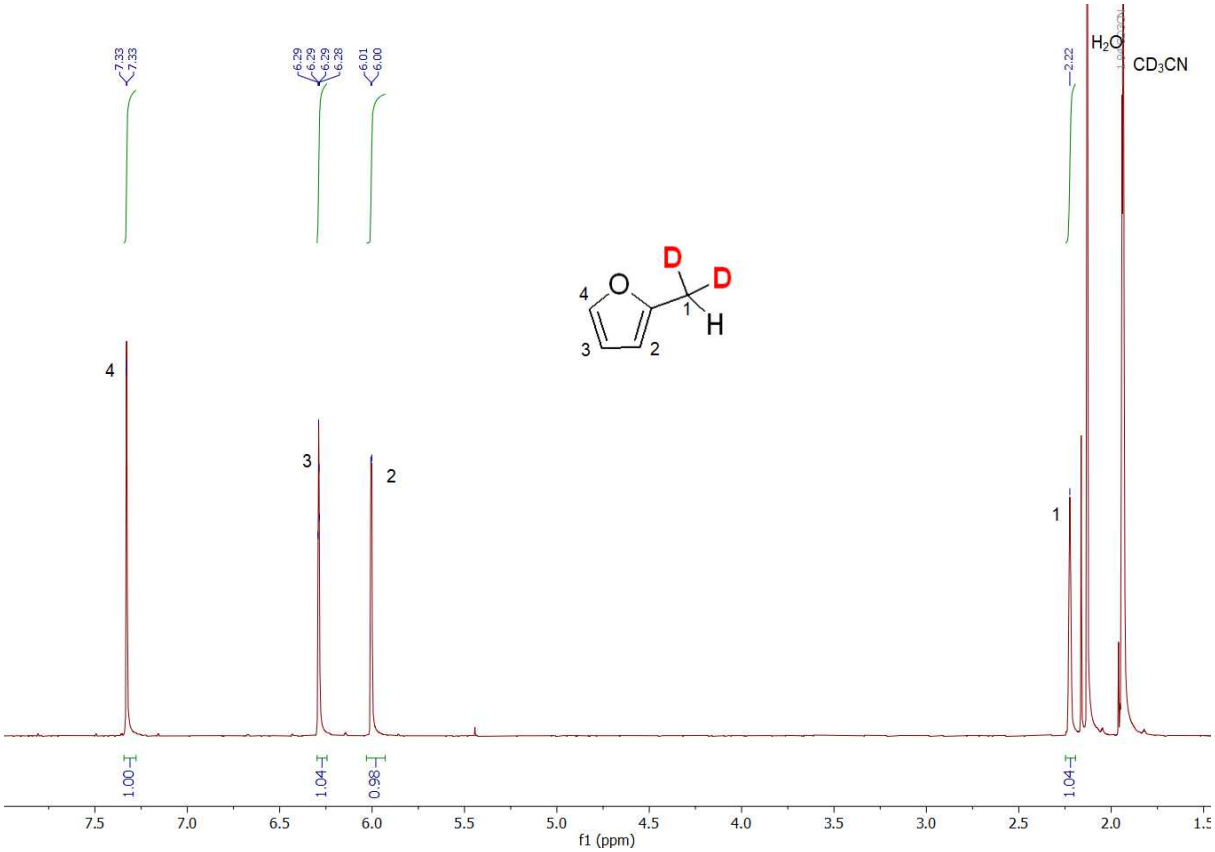

Figure S12. ^{1}H NMR test result of the trapping solution after electrolysis in D-only electrolyte. D-only electrolyte was prepared by dissoving 20 mM furfural in the electrolyte with 0.5 M D_2SO_4 in 1:3 (v/v) CD_3CN/D_2O co-solvent. The 1-hour electrolysis was performed on Pb foil at −1.20 V_{RHE}. The solution in trapping of the volatile MF was CD_3CN solvent in ice-water bath (**Figure S1**). The peak area ratios in the position 1, 2, 3, and 4 are 1.04:0.98:1.04:1.00, respectively.

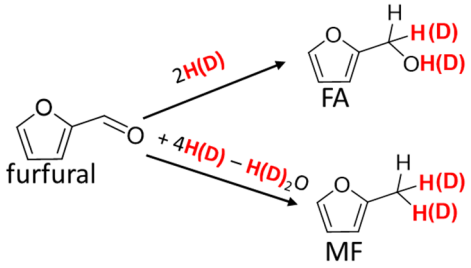

Figure S13. Identification of hydrogenation/deuteration pathway by ^{1}H NMR. Based on the ^{1}H-NMR test results from **Figure S5-S12**, FA is formed by addition of one H/D to the hydroxyl group and the other to the carbonyl carbon. MF is produced by adding both H/D to the alkyl group followed by C-O scission to remove one H_2O/D_2O molecule.

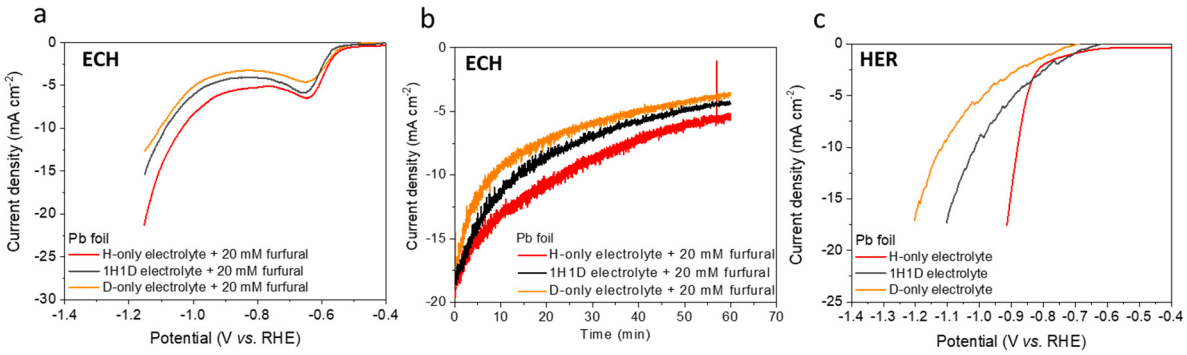

Figure S14. Electrolysis in H-only, 1H1D, and D-only electrolytes. (a) LSV curves, and (b) current-density-time profiles for electrolysis of 20 mM furfural-containing electrolyte. (c) LSV curves of HER. The constant potential test in (b) was performed at −1.20 V_{RHE} for 1 hour.

Supporting information note 2: Isotopic incorporation studies (Table S6-S12, Figure S15-S20)

(1) Calculation of the fraction of H/D in the products FA and MF

Table S6. GC-MS result of the sample after 1-hour electrolysis at −1.20 V_{RHE} in 1H1D electrolyte.

Reaction Condition	Fragment of FA (m/z)	Abundance (a.u.)	Percentage (%)	Fragment of MF (m/z)	Abundance (a.u.)	Percentage (%)
20 mM furfural 1H1D electrolyte	95	1168	5.40	81	23713	18.30
	96	453	2.10	82	50759	39.18
	97	4658	21.55	83	40922	31.58
	98	9685	44.82	84	13329	10.29
	99	5392	24.95	85	841	0.65
	100	255	1.18	86	0	0.00
Total		21611	100		129564	100

The isotope composition, specifically the fraction of D (f_D) and H (f_H) in the products, was calculated by solving two binary linear equations as follows:

$$S_a = f_H \times S_{Ha} + f_D \times S_{Da}$$

$$S_b = f_H \times S_{Hb} + f_D \times S_{Db}$$

where S_a and S_b represent the relative abundance (percentage) of MS signals at the m/z value of a and b, respectively, for the products (i.e., FA and MF) after electrolysis. Similarly, S_{Ha} and S_{Hb}, and S_{Da} and S_{Db} correspond to the same m/z values of products after electrolysis with 20 mM furfural in H-only and D-only electrolytes, respectively, as shown in **Table S1 and S3**.

(1-a) Calculation of the fraction of H/D in FA

The relative abundance of mass-to-charge ratio (m/z) is detected by GC-MS through the ionized molecules or their fragments. Therefore, the tested m/z signals are not a constant value and should be dispersedly

distributed in a range. Indeed, we obtained the m/z signals for FA are distributed in a wide range (mainly from 97 to 100), therefore we chose multiple m/z values to fit in the model for calculations. After calculations, regardless of the chosen m/z, the calculated S_a and S_b are close to similar values, which suggested the accuracy of this model. The detailed calculations are shown in (i)-(iv) as follows:

(i) If we use m/z values of **97 + 98** and **99 +100** to represent S_{Ha} and S_{Hb}, respectively, as shown in **Table S1**, the corresponding relative abundances (percentage) are equal to 88.26 and 3.31.

Similarly, from **Table S3,** S_{Da} and S_{Db} are 30.92 and 63.88, respectively.

For the FA sample after the electrolysis of 1H1D electrolyte, $S_a = 66.37$ and $S_b = 26.13$.

Then the two binary linear equations are as follows:

$66.37 = f_H \times 88.26 + f_D \times 30.92$

$26.13 = f_H \times 3.31 + f_D \times 63.88$

As a result, the solved $f_H = 0.62$ and $f_D = 0.38$.

If we sum f_H and f_D, it equals 1.00, which suggested the accuracy of this model.

(ii) If we use m/z values of **97 and 98** in the model, from **Table S1 and S3,** we obtained $S_{Ha} = 30.25$, $S_{Hb} = 58.02$, $S_{Da} = 7.02$, $S_{Db} = 23.90$.

Also, $S_a = 21.55$ and $S_b = 44.82$.

By substitution, the two binary linear equations are shown as follows:

$21.55 = f_H \times 30.25 + f_D \times 7.02$

$44.82 = f_H \times 58.02 + f_D \times 23.90$

As a result, the solved $f_H = 0.63$ and $f_D = 0.33$.

If we calculate $f_H + f_D$, it equals 0.96, which also suggested the accuracy of this model.

(iii) Similarly, if we use m/z values of **98 and 99** in the model, from **Table S1 and S3,** we got the $S_{Ha} = 58.02$, $S_{Hb} = 3.26$, $S_{Da} = 23.90$, $S_{Db} = 59.80$.

Also, $S_a = 44.82$ and $S_b = 24.95$.

Then,

$44.82 = f_H \times 58.02 + f_D \times 23.90$

$24.95 = f_H \times 3.26 + f_D \times 59.80$

The solved f_H is 0.62 and f_D is 0.38. The same value of $f_H + f_D = 1.00$ was obtained.

(iv) If we use m/z values of **97 and 99** in the model, from **Table S1 and S3,** we got the $S_{Ha} = 30.25$, $S_{Hb} = 3.26$, $S_{Da} = 7.02$, $S_{Db} = 59.80$.

Also, $S_a = 21.55$ and $S_b = 24.95$.

Then,

$21.55 = f_H \times 30.25 + f_D \times 7.02$

$24.95 = f_H \times 3.26 + f_D \times 59.80$

As a result, the solved $f_H = 0.62$ and $f_D = 0.38$. The same value of $f_H + f_D = 1.00$ was obtained.

(1-b) Calculation of the fraction of H/D in MF

The calculation of the fraction of H/D in MF is similar as FA. From the GC-MS results as shown in **Table S1 and S3**, we obtained the m/z values for MF is mainly in 81 + 82 (with a percentage ratio of 96.06%) for H-only electrolyte and 83 + 84 (with a percentage ratio of 75.45%) for D-only electrolyte.

Therefore, we used m/z percent ratio of 81 + 82 and 83 + 84 to represent S_{Ha} (equal to 96.06) and S_{Hb} (equal to 3.94), respectively. Similarly, $S_{Da} = 13.89$ and $S_{Db} = 75.45$. Also, $S_a = 57.48$ and $S_b = 41.87$.

$57.48 = f_H \times 96.06 + f_D \times 13.88$

$41.87 = f_H \times 3.94 + f_D \times 75.45$

As a result, the solved $f_H = 0.52$ and $f_D = 0.53$.

If we calculate $f_H + f_D$, it equals 1.05, which confirmed the accuracy of this model.

(2) H/D distribution analysis

fraction of H-H product = f_H^2

fraction of H-D product = $2 \times f_H \times f_D$

fraction of D-D product = f_D^2

After substitution of the obtained f_H and f_D in 1H1D electrolyte into the binomial equation.

(3) Accuracy analysis

If we substitute another GC-MS result after the electrolysis in H-only electrolyte (as shown in **Table S7** and substitute into the above model, we can get the fraction of H/D in FA and MF as follows:

Table S7. GC-MS result of the sample after 1-hour electrolysis at −1.20 V_{RHE} in H-only electrolyte.

Reaction Condition	Fragment of FA (m/z)	Abundance (a.u.)	Percentage (%)	Fragment of MF (m/z)	Abundance (a.u.)	Percentage (%)
20 mM furfural 0.5 M **H_2SO_4** 1:3 (v/v) **CH_3CN/H_2O**	95	1772	6.16	81	15875	37.42
	96	713	2.48	82	25122	59.22
	97	8866	30.81	83	1423	3.35
	98	16492	57.30	84	0	0
	99	937	3.26	85	0	0
	100	0	0	86	0	0
Total		28780	100		42420	100

For FA, we used the GC-MS result of 97 + 98 and 99 + 100, from the results in **Table S1, Table S3, and Table S7,** the calculations are shown as follows:

$88.11 = f_H \times 88.27 + f_D \times 30.92$

$3.26 = f_H \times 3.26 + f_D \times 63.88$

We got the $f_H = 1.00$ and $f_D = 0.00$ for FA.

For MF, we used the GC-MS result of 81 + 82 and 83 + 84 and calculated as follows:

$96.65 = f_H \times 96.06 + f_D \times 13.89$

$3.35 = f_H \times 3.94 + f_D \times 75.45$

We got the $f_H = 1.01$ and $f_D = 0.00$ for MF.

The above results confirmed the accuracy of the model used for isotopic incorporation studies.

(4) Control experiments

(i) Different concentrations of FA and MF

Table S8. GC-MS result of different concentrations of FA in CH_3CN solvent.

C_{FA} (mM)	10		5		2.5		1.25	
Fragment of FA (m/z)	Abundance (a.u.)	Percentage (%)	Abundance (a.u.)	Percentage (%)	Abundance (a.u.)	Percentage (%)	Abundance (a.u.)	Percentage (%)
95	73332	**4.49**	38531	**4.76**	19865	**5.03**	10219	**5.23**
96	19314	**1.18**	12100	**1.49**	7045	**1.78**	4154	**2.13**
97	507116	**31.08**	248527	**30.71**	120714	**30.54**	60132	**30.76**
98	970520	**59.49**	479685	**59.26**	232890	**58.91**	113764	**58.20**
99	56056	**3.44**	27827	**3.44**	13614	**3.44**	6553	**3.35**
100	5192	**0.32**	2724	**0.34**	1173	**0.30**	651	**0.33**
Total	163153	100	809394	100	395301	100	195473	100

Table S9. GC-MS result of different concentrations of MF in CH_3CN solvent.

C_{FA} (mM)	10		5		2.5		1.25	
Fragment of MF (m/z)	Abundance (a.u.)	Percentage (%)	Abundance (a.u.)	Percentage (%)	Abundance (a.u.)	Percentage (%)	Abundance (a.u.)	Percentage (%)
81	877334	**37.08**	370523	**37.01**	228324	**37.13**	115590	**37.00**
82	1402503	**59.27**	593836	**59.31**	364590	**59.29**	185380	**59.34**
83	81340	**3.44**	34824	**3.48**	20950	**3.41**	10849	**3.47**
84	4920	**0.21**	2073	**0.21**	1048	**0.17**	561	**0.18**
85	0	**0**	0	**0**	0	**0**	0	**0**
86	0	**0**	0	**0**	0	**0**	0	**0**
Total	2366097	100	1001256	100	614912	100	312380	100

From GC-MS results in **Table S8 to S9,** the relative percentage at different m/z values for both FA and MF are independent of their concentrations.

(5) H-D exchange

To confirm that the reactant and products do not exchange protons appreciably with deuterium in solutions, 10 mM furfural, FA, and MF were dissolved separately in fully deuterated solutions (D-only electrolyte) and placed for 1.5 h (longer than the electrolysis time of 1 h). From GC-MS results in **Table S10-S12** as follows, no notable incorporation of D was observed.

Table S10. GC-MS result of 10 mM furfural in D-only electrolyte for different standing durations.

Time (h)	0.5		1.5	
Fragment of furfural (m/z)	Abundance (a.u.)	Percentage (%)	Abundance (a.u.)	Percentage (%)
94	27	**0**	65	**0**
95	1442570	**48.02**	1465279	**48.07**
96	1465968	**48.79**	1484759	**48.71**
97	87683	**2.92**	89669	**2.94**
98	7818	**0.26**	8175	**0.27**
99	297	**0.01**	297	**0.01**
Total	3004363	100	3048244	100

Table S11. GC-MS result of 10 mM FA in D-only electrolyte for different standing durations.

Time (h)	0.5		1.5	
Fragment of furfural (m/z)	Abundance (a.u.)	Percentage (%)	Abundance (a.u.)	Percentage (%)
95	55364	**4.27**	57007	**4.30**
96	12660	**0.98**	13567	**1.02**
97	406698	**31.35**	407193	**30.68**
98	771772	**59.50**	794232	**59.85**
99	46490	**3.58**	50344	**3.79**
100	4171	**0.32**	4704	**0.35**
Total	1297155	100	1327047	100

Table S12. GC-MS result of 10 mM MF in D-only electrolyte for different standing durations.

Time (h)	0.5		1.5	
Fragment of furfural (m/z)	Abundance (a.u.)	Percentage (%)	Abundance (a.u.)	Percentage (%)
81	583485	37.08	576724	37.08
82	932268	59.24	921517	59.25
83	54479	3.46	53649	3.45
84	3375	0.21	3285	0.21
85	0	0	17	0
86	0	0	0	0
Total	1297155	100	1555192	100

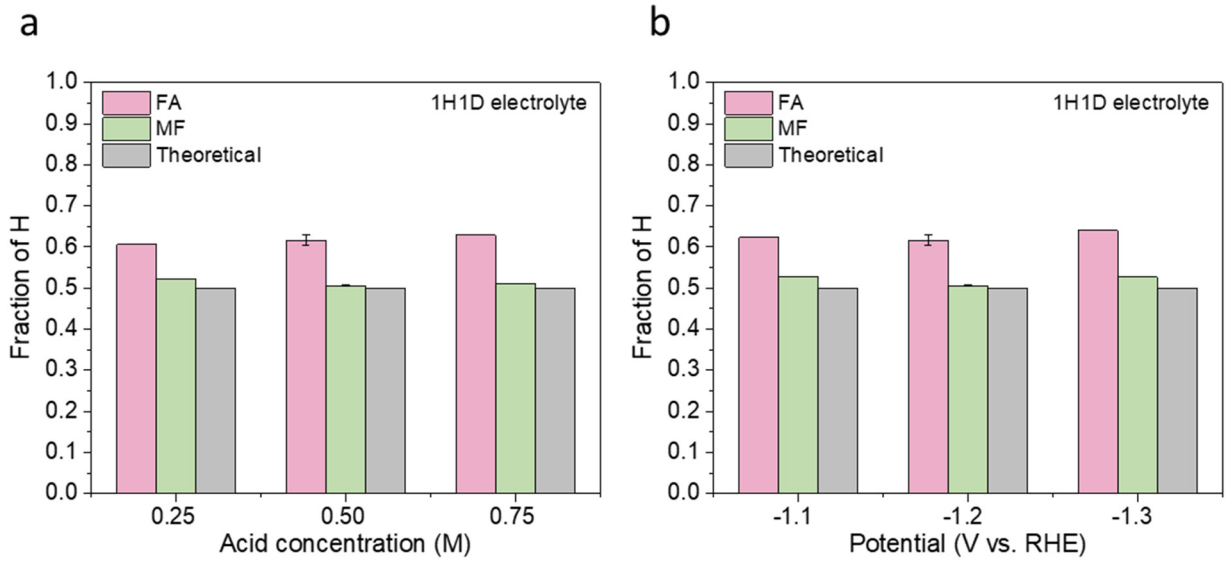

Figure S15. Fraction of H in (a) different concentration of acid and (d) different potentials on Pb foil. The electrolysis was performed in 1H1D electrolyte with 20 mM furfural at −1.20 V_{RHE} for 1 h.

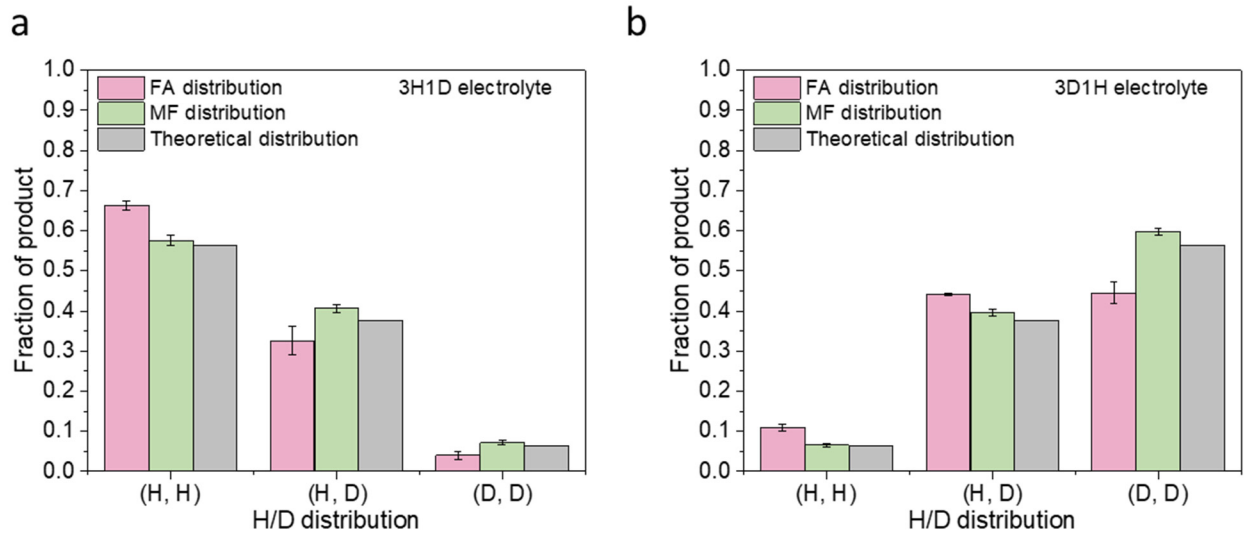

Figure S16. H/D distribution in FA and MF after the electrolysis of (a) 3H1D and (b) 1H3D electrolytes on Pb foil. The electrolysis was performed at −1.20 V_{RHE} for 1 h.

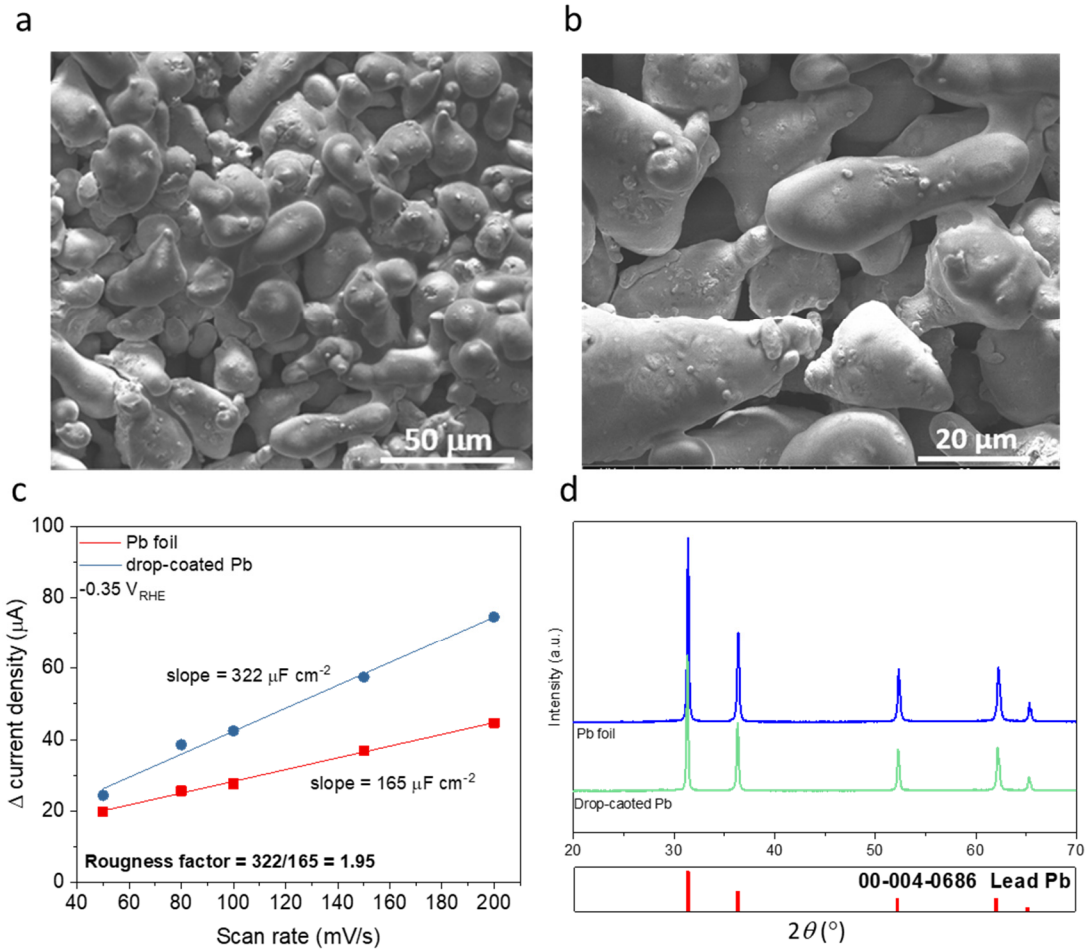

Figure S17. Characterization of drop-coated Pb. (a)-(b) SEM images. (c) Roughness factor. Roughness factor is calculated from the electrochemical surface area (ECSA) ratio of drop-coated Pb and Pb foil, which is estimated from the double layer charging/discharging current at different scan rates. (d) XRD patterns. XRD results showed polycrystalline Pb for both Pb foil and drop-coated Pb.

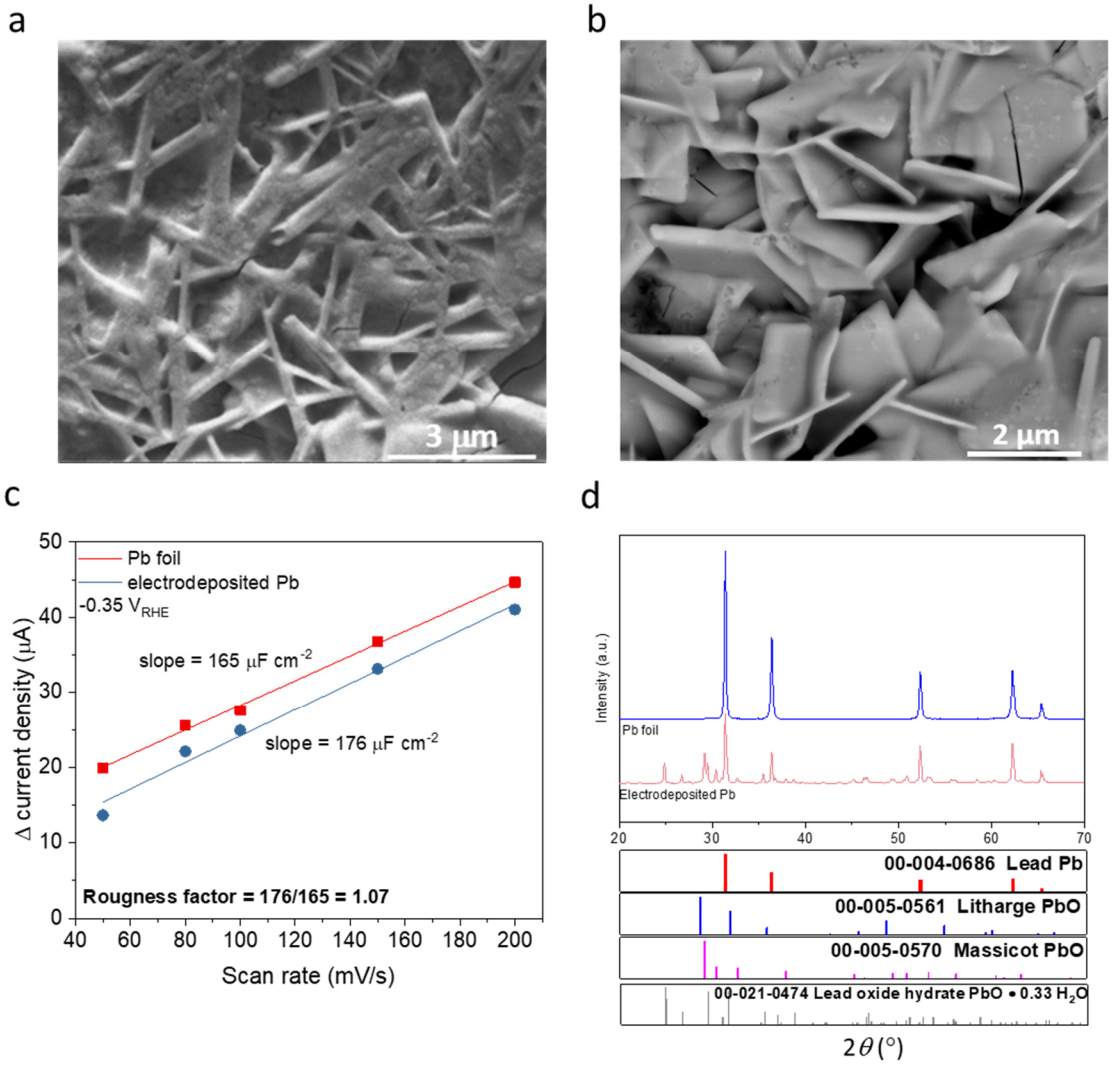

Figure S18. Characterization of electrodeposited Pb. (a)-(b) SEM images. (c) roughness factor. (d) XRD patterns. XRD results showed three different types of lead oxide on electrodeposited Pb.

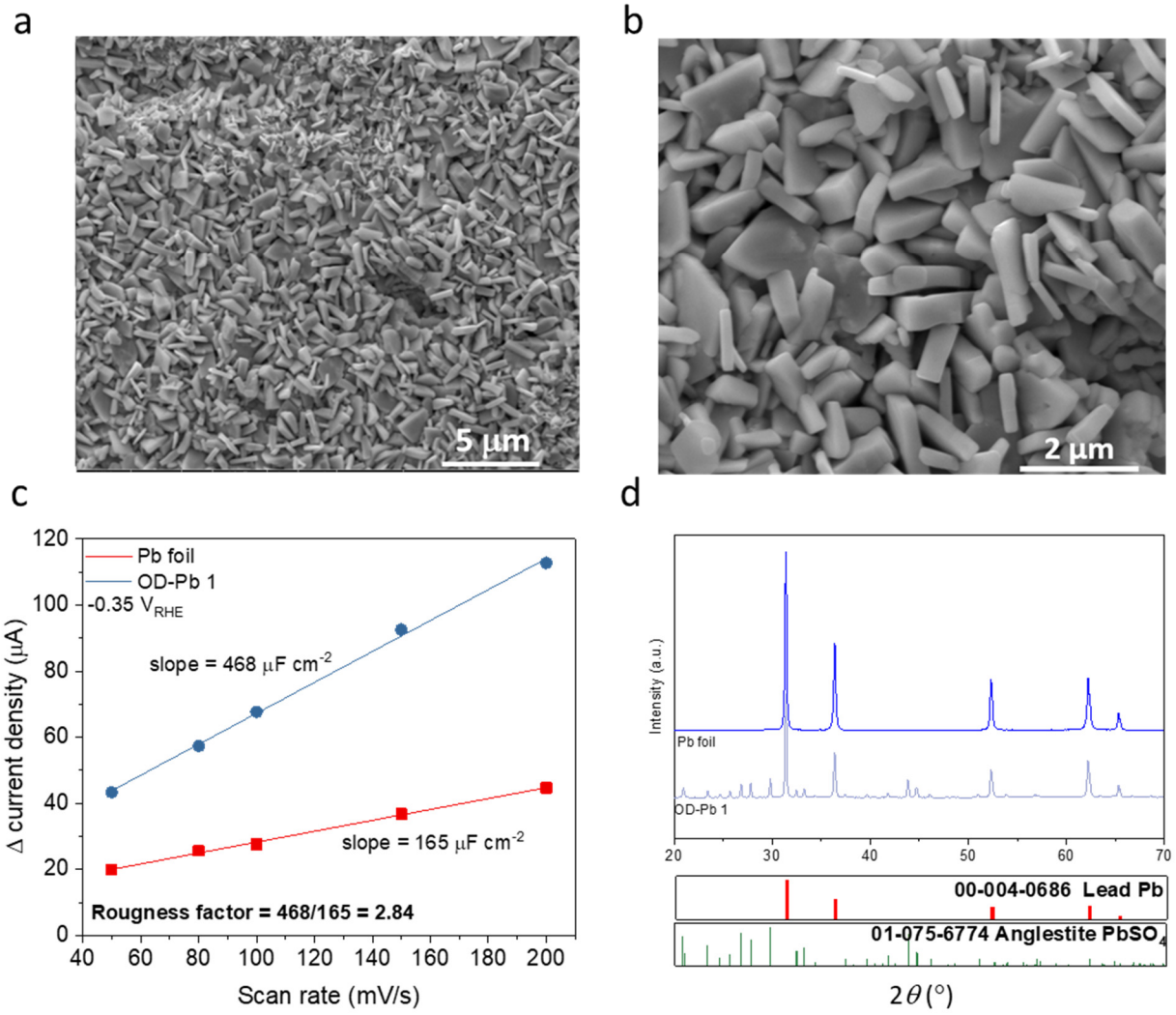

Figure S19. Characterization of OD-Pb-1. (a)-(b) SEM images. (c) roughness factor. (d) XRD patterns. XRD results showed $PbSO_4$ phase on OD-Pb-1.

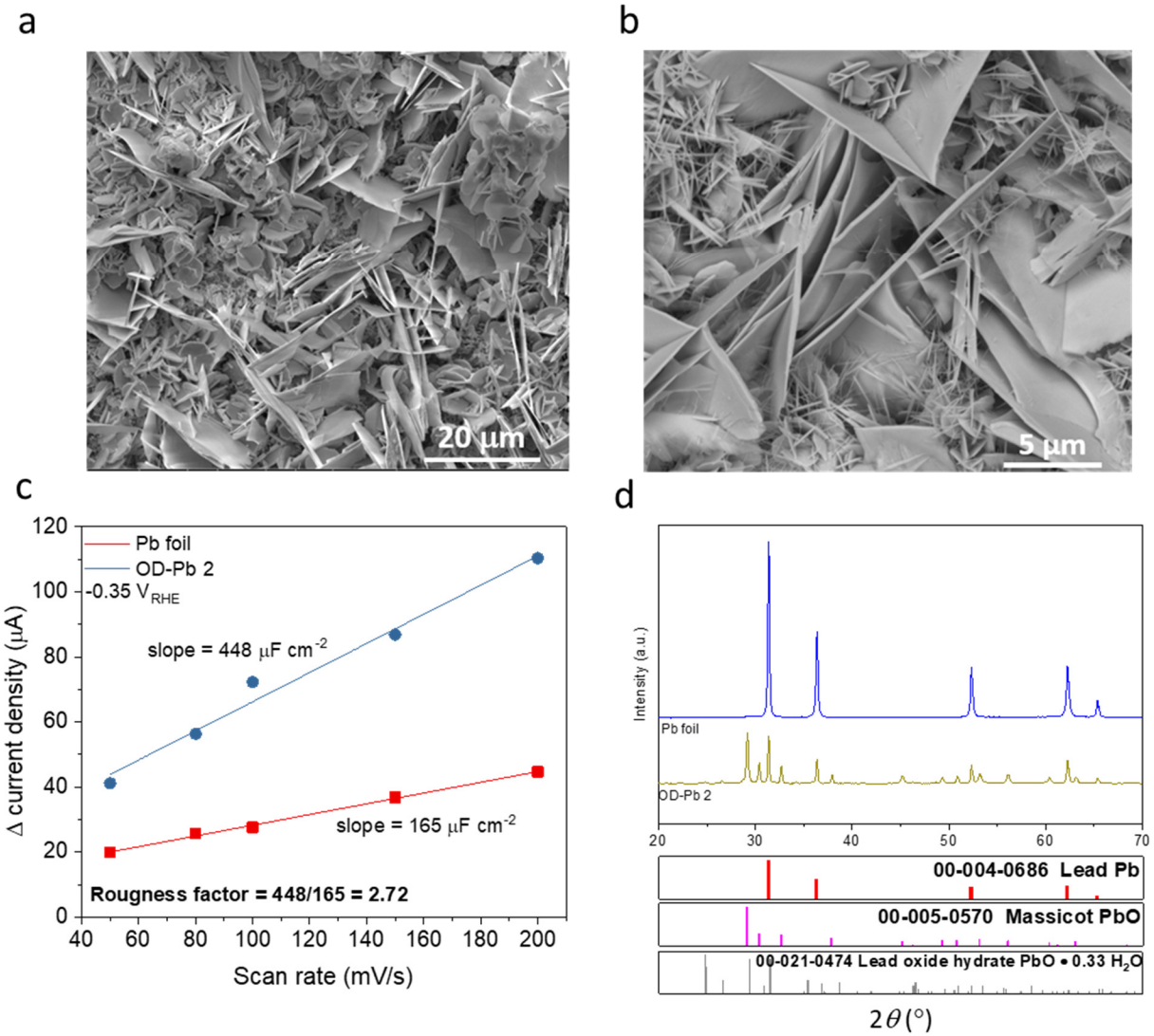

Figure S20. Characterization of OD-Pb-2. (a)-(b) SEM images. (c) roughness factor. (d) XRD patterns. XRD showed two types of lead oxide phases on OD-Pb-2.

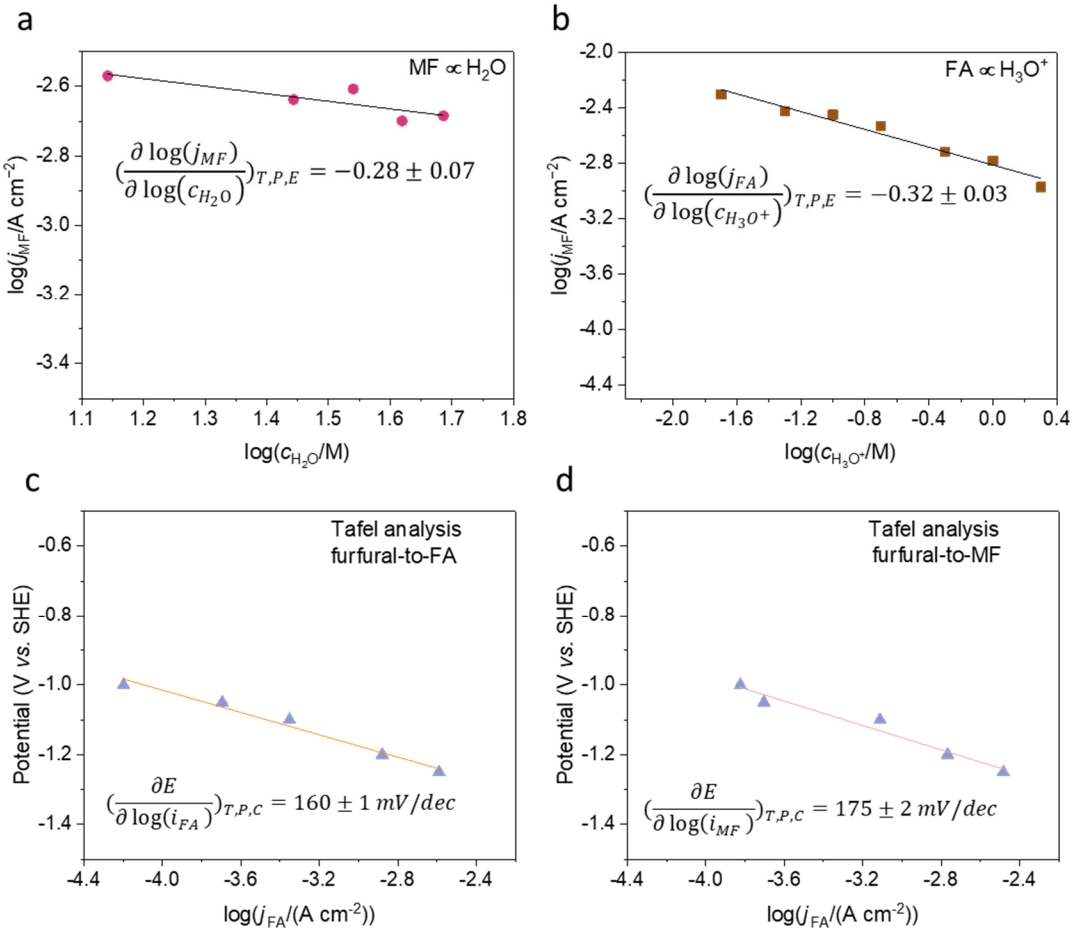

Figure S21. Electrokinetic studies for ECH of furfural on Pb foil. (a) Dependence of partial current density of MF on H_2O concentration. (b) Dependence of partial current density of FA on H_3O^+ concentration. The electrolysis was performed on Pb foil with applied charge of 60 C at −1.20 V_{SHE} with 20 mM furfural in the electrolyte. (c)-(d) Tafel analysis for furfural-to-FA and furfural-to-MF reactions. The electrolysis was performed on Pb foil with applied charge of 60 C at different potentials from −1.00 to −1.25 V_{SHE}.

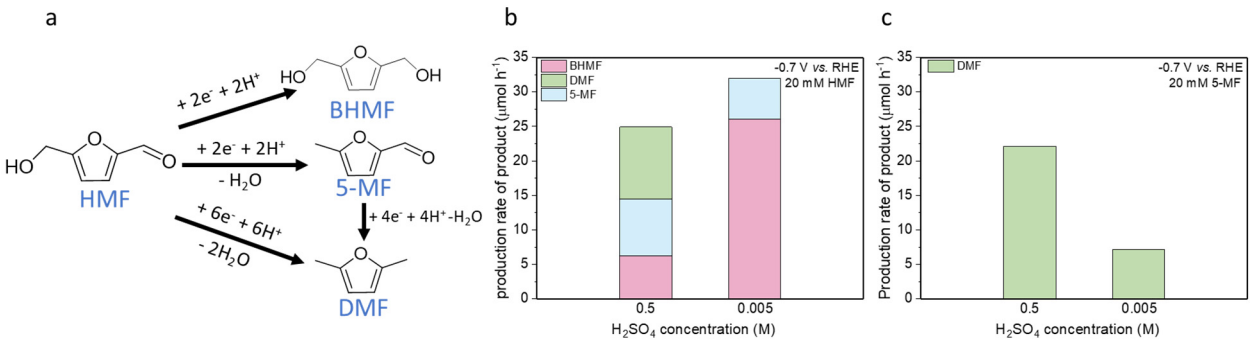

Figure S22. CA tests of HMF and 5-MF on Ag foil under acidic conditions. (a) Proposed reductive pathways from HMF to BHMF, 5-MF, and DMF. (b)-(c) Production rate at −0.7 V_{RHE} for 1-hour electrolysis of (b) 20 mM HMF or (c) 20 mM 5-MF with different concentrations of H_2SO_4. HMF was dissolved in the electrolyte with 0.5 M H_2SO_4 and 1:3 (v/v) CH_3CN/H_2O co-solvent. The electrolyte ionic strength was maintained at a constant value of 0.5 M (H_2SO_4 + Na_2SO_4 = 0.5 M).

a

pH	Buffer system
3	Citrate-Phosphate
5	Citrate-Phosphate
7	Phosphate
9	Borate
11	$NaHCO_3$-NaOH

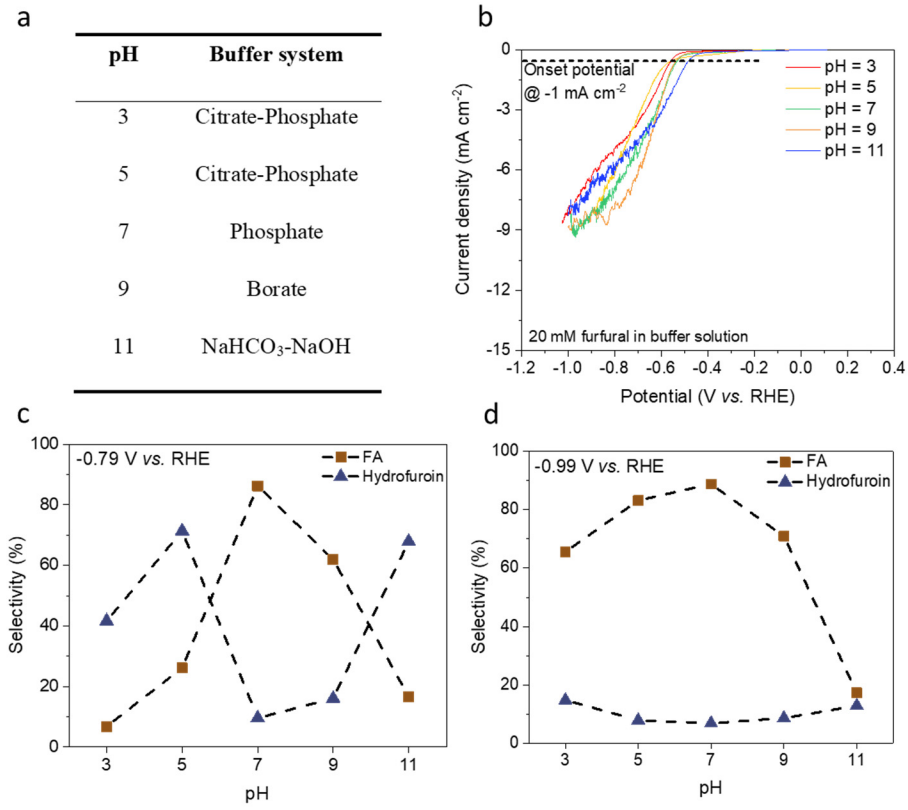

Figure S23. ECH of furfural in different buffer solutions at pH ranging from 7-11. (a) Different buffer systems with varying pH. (b) LSV curves on different buffer solutions with 20 mM furfural. (c)-(d) CA tests in different buffer solutions for 1-hour at −0.79 V_{RHE} and −0.99 V_{RHE} with 20 mM furfural.

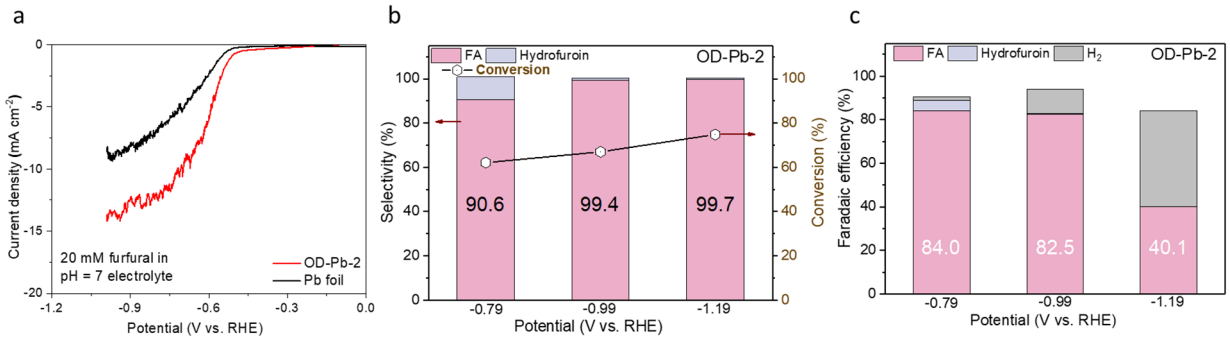

Figure S24. ECH of furfural on OD-Pb-2. (a) LSV curves on Pb foil and OD-Pb-2. (b) Product selectivity and conversion, and (c) Faradaic efficiency of product on OD-Pb-2. The electrolysis was performed in pH = 7 buffer solution with 20 mM furfural.

Supporting information, note 3: Derivative equations for Langmuir-Hinshelwood and Eley-Rideal mechanisms

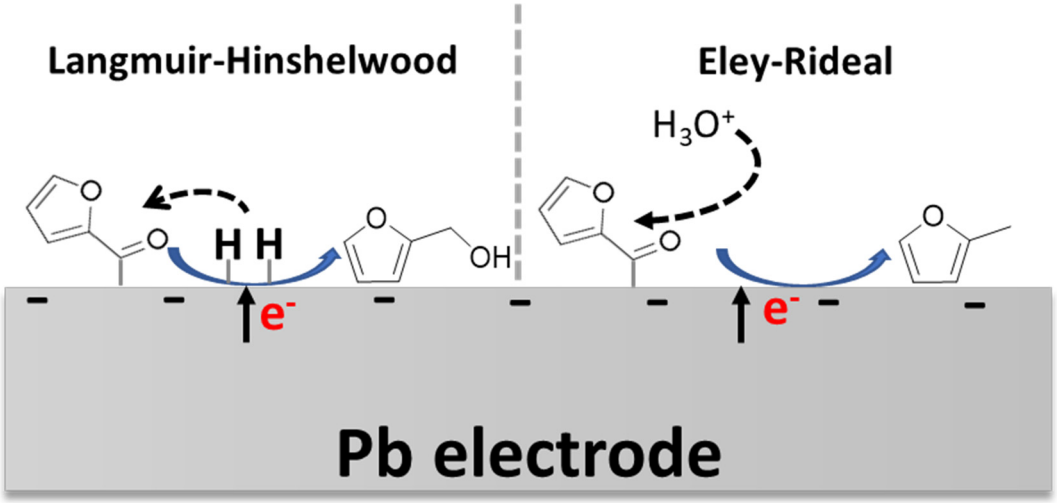

Figure S25. Simplified Scheme of Langmuir-Hinshelwood and Eley-Rideal mechanisms for FA and MF formation, respectively.

The derivation of rate constant was modified based on a previous work for ECH of benzaldehyde.[36]
From the site balance on the Pb surface,

$$[*_{tot}] = [*] + [\mathrm{Fur}^*] + [\mathrm{H}^*]$$

$$\frac{[*_{tot}]}{[*_{tot}]} = \frac{[*] + [\mathrm{Fur}^*] + [\mathrm{H}^*]}{[*_{tot}]} \rightarrow 1 = \theta + \theta_{\mathrm{Fur}} + \theta_H$$

Where [*tot] represents the total surface sites, [Fur*] and [H*] represent the surface sites occupied by furfural and H, respectively, and [*] represent the unoccupied sites. θ represents the fraction of the corresponding covered and uncovered surface sites.

To simplify the analysis, we assumed the adsorption of furfural species only occupied one site.[36] In addition, based on the electrochemical test condition at very negative potentials with a large current density, we assumed competitive adsorption of the surface sites with no empty sites.

$$1 = \theta_{\mathrm{Fur}} + \theta_{\mathrm{H}}$$

$$\theta_{\mathrm{Fur}} = \frac{[\mathrm{Fur}^*]}{[*_{tot}]} = \frac{[\mathrm{Fur}^*]}{[*] + [\mathrm{Fur}^*] + [\mathrm{H}^*]}$$

$$\theta_{\mathrm{H}} = \frac{[\mathrm{H}^*]}{[*_{tot}]} = \frac{[\mathrm{H}^*]}{[*] + [\mathrm{Fur}^*] + [\mathrm{H}^*]}$$

If we assume the adsorption and desorption of furfural and H are both at equilibrium, then,

$$\mathrm{v}_{\mathrm{ads,Fur}} = \mathrm{v}_{\mathrm{des,Fur}}$$

$$\mathrm{k}_{\mathrm{ads,Fur}} \times [\mathrm{Fur}] \times [*] = \mathrm{k}_{\mathrm{des,Fur}} \times [\mathrm{Fur}^*]$$

$$[\mathrm{Fur}^*] = \frac{\mathrm{k}_{\mathrm{ads}} \times [\mathrm{Fur}] \times [*]}{\mathrm{k}_{\mathrm{des}}} = \mathrm{K}_{\mathrm{Fur}} \times [\mathrm{Fur}] \times [*]$$

where $\mathrm{v}_{\mathrm{ads,Fur}}$ and $\mathrm{v}_{\mathrm{des.Fur}}$ represent the rate of furfural adsorption and desorption, respectively. [Fur] is the furfural concentration in the electrolyte, and $\mathrm{K}_{\mathrm{Fur}}$ represents the adsorption/desorption equilibrium constant of furfural.

Similarly, for the adsorption of hydrogen,

$$\mathrm{v}_{\mathrm{ads,H}} = \mathrm{v}_{\mathrm{des,H}}$$

$$\mathrm{k}_{\mathrm{ads,H}} \times a_{H_3O^+} \times [*] = \mathrm{k}_{\mathrm{des,H}} \times [\mathrm{H}^*]$$

$$[\mathrm{H}^*] = \frac{\mathrm{k}_{\mathrm{ads,H}} \times a_{H_3O^+} \times [*]}{\mathrm{k}_{\mathrm{des,H}}} = K_{\mathrm{H}} \times a_{H_3O^+} \times [*]$$

where $\mathrm{v}_{\mathrm{ads,H}}$ and $\mathrm{v}_{\mathrm{des,H}}$ represent the rate of hydrogen adsorption and desorption, respectively. a_{H3O}^{+} represents proton concentration in the electrolyte, and K_{H} represents the adsorption/desorption equilibrium constant of proton.

Therefore,

$$\theta_{\mathrm{Fur}} = \frac{[\mathrm{Fur}^*]}{[*] + [\mathrm{Fur}^*] + [\mathrm{H}^*]} = \frac{K_{\mathrm{Fur}} \times [\mathrm{Fur}] \times [*]}{[*] + K_{\mathrm{Fur}} \times [\mathrm{Fur}] \times [*] + K_{\mathrm{H}} \times a_{H_3O^+} \times [*]}$$

$$= \frac{K_{\mathrm{Fur}} \times [\ \mathrm{Fur}\ ]}{1 + K_{\mathrm{Fur}} \times [\ \mathrm{Fur}\ ] + K_{\mathrm{H}} \times a_{H_3O^+}}$$

$$\theta_{\mathrm{H}} = \frac{[\mathrm{H}^*]}{[*] + [\mathrm{Fur}^*] + [\mathrm{H}^*]} = \frac{K_{\mathrm{H}} \times a_{H_3O^+} \times [*]}{[*] + K_{Fur} \times [\mathrm{Fur}] \times [*] + K_{\mathrm{H}} \times a_{H_3O^+} \times [*]}$$

$$= \frac{K_{\mathrm{H}} \times a_{H_3O^+}}{1 + K_{\mathrm{Fur}} \times [\ \mathrm{Fur}\ ] + K_{\mathrm{H}} \times a_{H_3O^+}}$$

(1) For the **Langmuir-Hinshelwood adsorption** with both furfural and hydrogen adsorbed on the electrode surface, we assumed the competitive adsorption of furfural and hydrogen on the Pb surface, and the

adsorption of first H is the rate-limiting step, which is reasonable based on the KIE observed from the main text.

Then, the reaction rate ($r_{\text{L-H}}$) can be found to have the form:

$$r_{L-H} = k_T \times \theta_{\text{Fur}} \times \theta_{\text{H}}$$

$$r_{L-H} = \frac{k_T \times K_{\text{Fur}} \times [\text{ Fur }] \times K_{\text{H}} \times a_{H_3O^+}}{\left(1 + K_{\text{Fur}} \times [\text{ Fur }] + K_{\text{H}} \times a_{H_3O^+}\right)^2}$$

Where k_{T} is the reaction rate constant.

At a low surface coverage (or low concentration) of furfural, $K_{\text{Fur}} \times [\text{Fur}] \ll 1$

$r_{L-H} \approx \frac{k_T \times K_{\text{Fur}} \times [\text{ Fur }] \times K_{\text{H}} \times a_{H_3O^+}}{\left(1 + K_{\text{H}} \times a_{H_3O^+}\right)^2}$, **positive order** on furfural concentration

At a high surface coverage (or high concentration) of furfural, $K_{\text{Fur}} \times [\text{Fur}] \gg 1$

$r_{L-H} \approx \frac{k_T \times K_{\text{H}} \times a_{H_3O^+}}{K_{\text{Fur}} \times [\text{ Fur }]}$, **negative order** on furfural concentration

(2) For the **Eley-Rideal** with furfural adsorbed on the surface and hydrogen originate from the electrolyte near the electrode/electrolyte interface, then the rate constant ($r_{\text{E-R}}$) should be,

$$r_{ER} = k_T \times \theta_{\text{Fur}} \times a_{H_3O^+}^n$$

n represents the reaction order with respect to the proton concentration (H_2O or H_3O^+) in the electrolyte, therefore,

$$r_{\text{E-R}} = \frac{k_{\text{T}} \times K_{\text{Fur}} \times [\text{Fur}] \times a_{H_3O^+}}{1 + K_{\text{Fur}} \times [\text{Fur}] + K_{\text{H}} \times a_{H_3O^+}}$$

At a low surface coverage (or low concentration) of furfural, $K_{\text{Fur}} \times [\text{Fur}] \ll 1$

$r_{E-R} \approx \frac{k_{\text{T}} \times K_{\text{Fur}} \times [\text{Fur}] \times a_{H_3O^+}}{1 + K_{\text{H}} \times a_{H_3O^+}}$, **positive order** on furfural concentration

At a high surface coverage (or high concentration) of furfural, $K_{\text{Fur}} \times [\text{Fur}] \gg 1$

$r_{E-R} \approx k_{\text{T}} \times a_{H_3O^+}$, **zero order** on furfural concentration

(3) Estimating maximum adsorption of furfural on polycrystalline Pb foil

The surface area of Pb exposed to the electrolyte is 2cm^2 ($1 \times 1\ \text{cm}^2$, two sides)

We roughly assumed the number of Pb atoms per cm^2 is the same with Pt, which is 1.3×10^{15}.[37]

Assume the monolayer coverage of furfural on the surface.

Total number of Pb atoms on the surface: $1.3 \times 10^{15} \times 2 = 2.6 \times 10^{15}$ atoms

The maximum surface coverage of furfural is assumed by one molecular furfural (C5 molecular) occupied five atoms of surface atoms of Pb surface. If the surface is saturated adsorbed by furfural, the moles of adsorbed furfural:

$$2.6 \times 10^{15} \text{ atoms of Pb} \times \frac{1 \text{ furfural molecule}}{5 \text{ Pb atoms}} \times \frac{1 \text{ mol furfural}}{6.02 \times 10^{23} \text{ furfural molecules}} = 8.6 \times 10^{-10} \text{ moles furfural}$$

In our reaction conditions all over the work, we used the minimal furfural concentration of 20 mM in 20 mL of electrolyte,

Then, the total moles of furfural in the electrolyte are,

$0.02 \times 0.02 = 4 \times 10^{-4}$ moles of furfural $>> 8.6 \times 10^{-10}$ moles of the maximum coverage

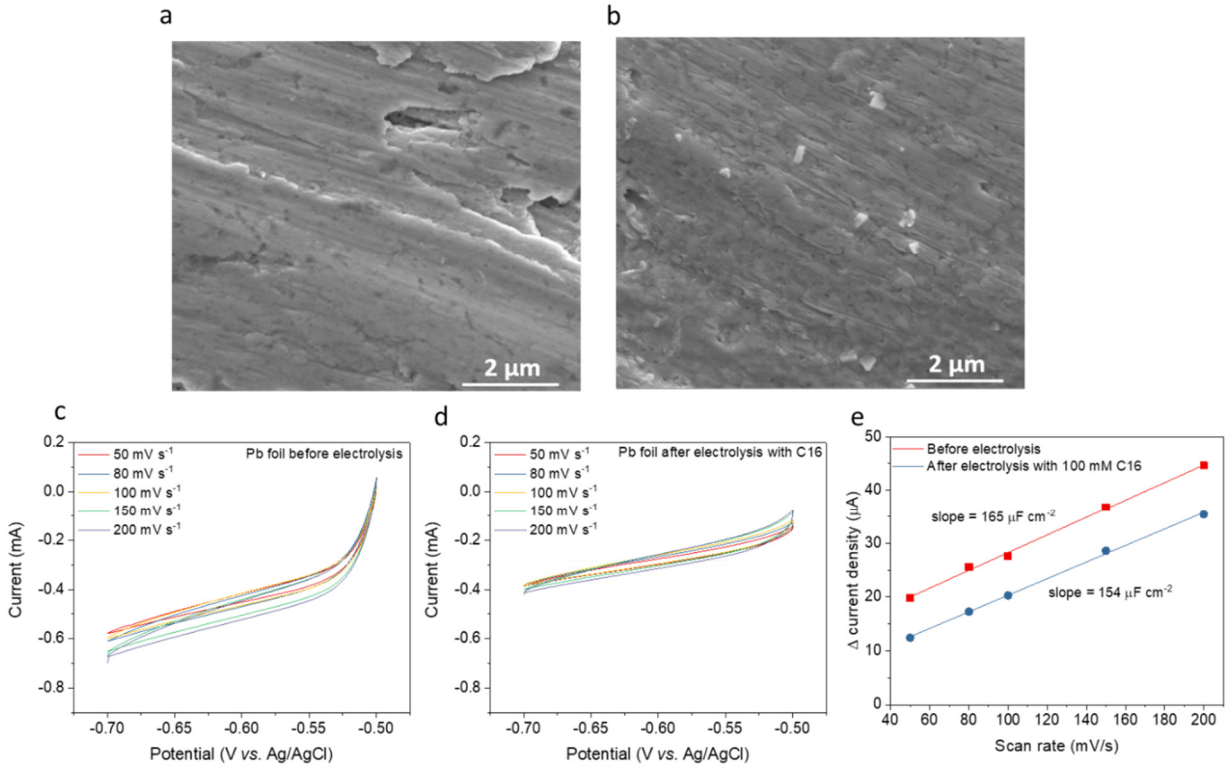

Figure S26. Pb surface characterization before and after electrolysis in the presence of cation surfactant. (a)-(b) SEM images and (c)-(e) double layer capacitance before and after the electrolysis in the presence of 100 mM C16. The electrolysis was performed on Pb foil at −1.20 V_{RHE} for 0.5 h. No significant changes in the morphology and surface area on Pb surfaces were observed after the electrolysis in the presence of C16.

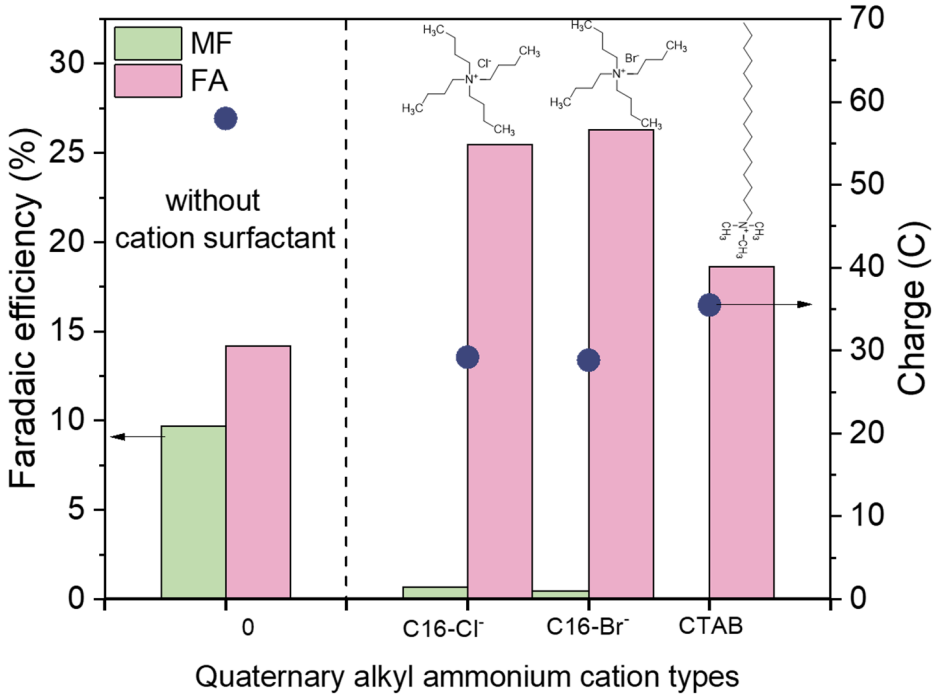

Figure S27. Control experiments of tailoring the double layer by different types of cations. The electrolysis was performed on Pb foil at −1.20 V_{RHE} for 0.5 h with or without 50 mM quaternary alkyl ammonium cations. Control experiments compared the coupled anions (Br^-or Cl^-) in C16, and an asymmetric cation of CTAB with 19 carbons. Inset of this figure is the chemical structures of these cation surfactants.

By changing the coupled anion from Cl^- to Br^- in the cationic surfactant (**Figure S27**), similar activity is still maintained, supporting the responsibility of cations in switching the selectivity. Also, when the symmetric long-chain alkyl groups in the above-used cations were replaced by an asymmetric tetraalkylammonium salt with 19 carbons (**Figure S27**),[38-39] namely cetyltrimethylammonium bromide (CTAB), a similar result of the increased FA and undetectable MF is obtained, as compared to the result without addition of CTAB. These results highlighted the radius and hydrophobic nature of cationic surfactant are indeed critical in modifying the local environments at the electrode interface, which have related local content of H_3O^+ and H_2O with the generation of MF and FA, respectively.

Supporting information, note 4: mathematic modeling electric filed

The altered local ΔpH can be elaborated mathematically through a model to correlate ΔpH with the electrostatic potentials inside double layer. Despite most charges of the electrode is confined on the surface, in the electrolyte it may take some thickness of solution to accumulate charge to counterbalance the surface charge. Based on the Gouy−Chapman−Stern (GCS) theory,[40] the electric field profile in the electrolyte is plotted in the main text. The differential capacitance inside the double layer (C_{dl}) comprised a series of network of Helmholtz layer (C_H) and diffusion-layer (C_D) capacitances. The local concentration of H_3O^+ at the compact OHP layer is denoted as $c_{H^+}^{CL}$, which is related to the concentration of H_3O^+ in the diffusion layer by Boltzmann equation as follows:

$$c_{H^+}^{CL} = c_{H^+}^{bulk} \exp\left(\frac{-e\varphi_{CL}}{kT}\right)$$

where φ_{CL} is the electrostatic potential (V) at the OHP plane, k is the Boltzmann constant (1.38×10^{-23} m^2 kg s^{-2} K^{-1}), e is the electron charge (1.60×10^{-19} C) and T is the absolute temperature (K). Taking the logarithm of the above equation yields,

$$pH_{CL} = pH_{bulk} + 0.43\frac{e\varphi_{CL}}{kT}$$

We used subscript ($_0$) and superscript (') when referring to the absence and presence of cation surfactants, respectively, and assumed their bulk pH are equal ($pH_{bulk0} = pH_{bulk}'$). By subtraction, we obtained the equations as follows:

$$\Delta pH = pH_{CL}' - pH_{CL0} = 0.43\frac{e(\varphi_{CL}' - \varphi_{CL0})}{kT}$$

$$59.9\,mV \times \Delta pH = \varphi_{CL}' - \varphi_{CL0} = \Delta\varphi$$

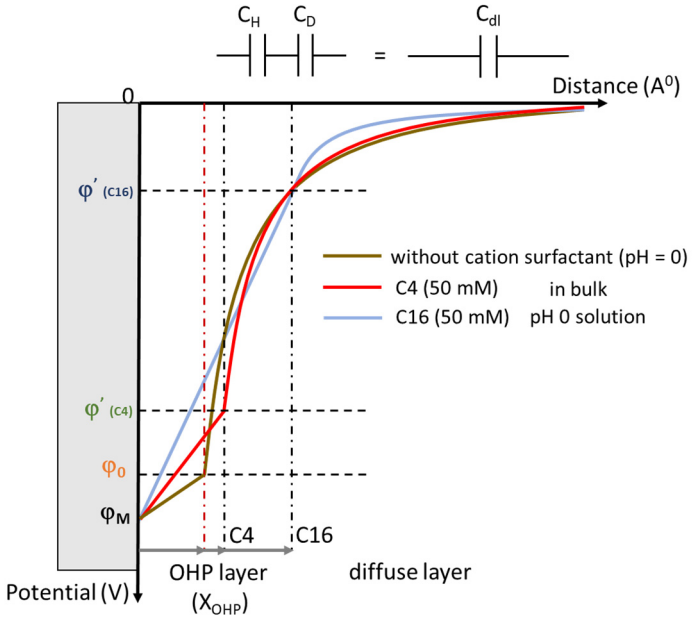

Figure S28. Diagram of the interfacial electrostatic potential profile modified by the cationic surfactants. With the addition of cationic surfactants (C4 or C16), the thickness of OHP layer (X_{OHP}) increased (right shifted) because of their larger radii as compared to the background H_3O^+. The double-layer capacitance

(C_{dl}) is divided into two regions in series: OHP layer (C_H) and diffusion layer (C_D). The corresponding capacitance relationship is $1/C_{dl} = 1/C_H + 1/C_D$.

Other than the change in local ΔpH, the concurrently altered electrostatic potentials at the solid-liquid interfaces can also play an important role in electrocatalysis.[41-42] A mathematic [40] was applied to correlate local ΔpH with the electrostatic potentials changes (Δφ) inside the double layer, exhibiting a Nernstian shift (~60 mV per ΔpH) of Δφ with respective to the local ΔpH. Therefore, with the four cationic surfactants examined, the calculated Δφ is varied from 47.3 to 100.0 mV. **Figure S28** plotted the C4 and C16 results as examples and compared them with the curve in pH 0 electrolyte without cationic surfactant. Based on the GCS model, the potential profile in the OHP and diffusion layers are linear and exponential, respectively. It should be noted that, at a given bulk pH (= 0) and electrochemical potential (E = −1.20 V_{RHE}), the electrostatic potential at the electrode surface (φ_M) is a constant, irrespective of the interfacial pH and ionic strength.[42] Considering a systematical increase in radius of cation surfactants compared to the background ions ($H_3O^+ \approx Na^+$)[40, 43] < C4 < C8 < C12 < C16,[44] the cations arranged in the compact OHP layer (x_{OHP}, the distance between the electrode surface and a plane of the closest distance from the centers of ions) thus shifted away from the electrode surface.

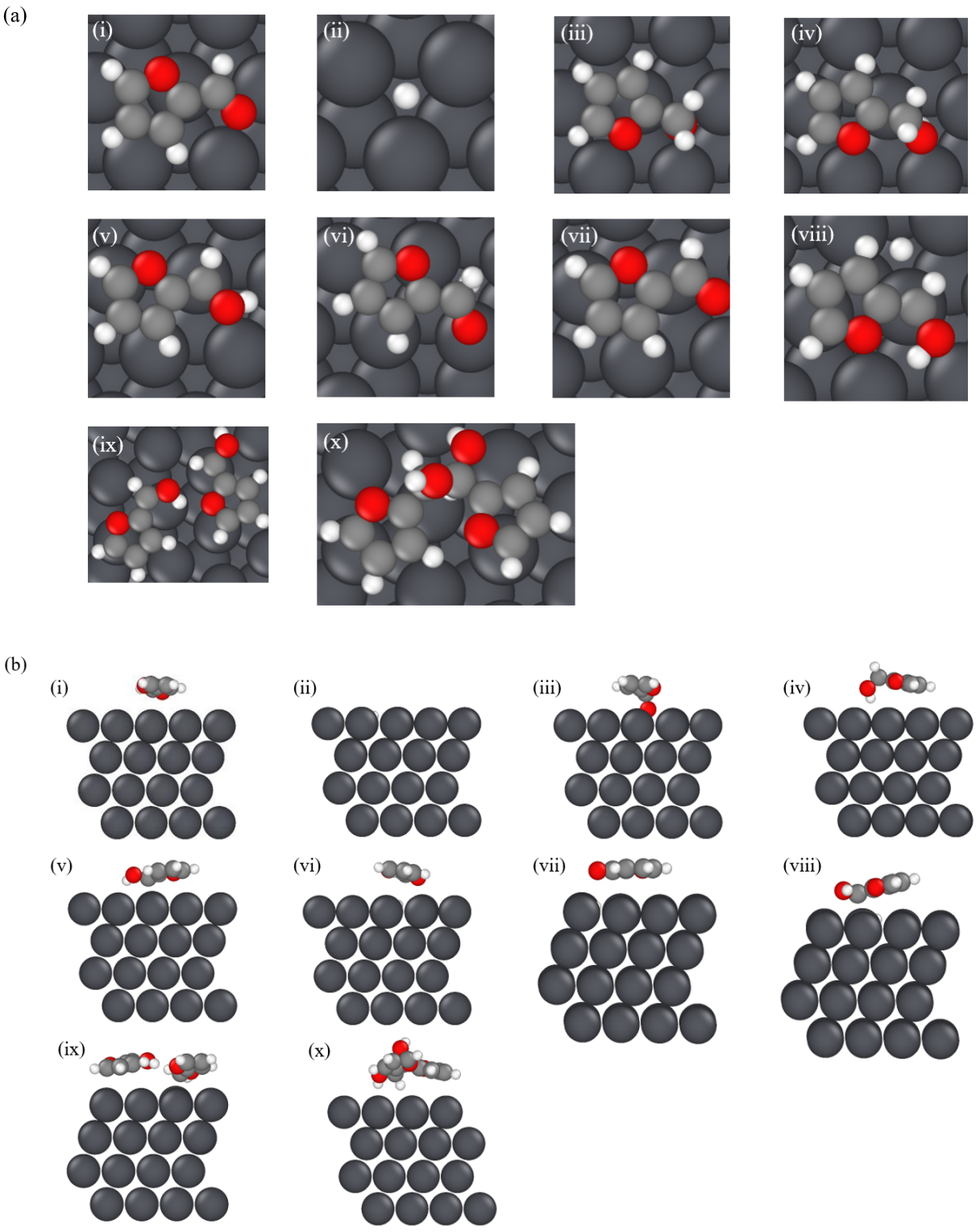

Figure S29. (a) Top view, and (b) side view of most stable binding geometries of considered reaction intermediates on Pb(111). (i) FUR-CHO* (furfural*), (ii) H*, (iii) FUR-CH_2O*, (iv) FUR-CH_2OH*

(furfuryl alcohol* (FA*)), (v) FUR-CHOH* (ketyl radical*), (vi) FUR-CHO* + H* (initial state (IS) for NEB/CI-NEB calculations for FUR-CH_2O* formation step), (vii) FUR-CHOH* + H* (IS for NEB/CI-NEB calculations for ketyl radical* formation step), (viii) FUR-CHOH* + H* (IS for NEB/CI-NEB calculations for FA* formation step), (ix) FUR-CHOH* + FUR-CHOH* (IS for NEB/CI-NEB calculations for HF* formation step), (x) $(FUR\text{-}CHOH)_2$* (hydrofuroin* (HF*)). In species naming, FUR denotes the furan ring, and * denotes an adsorbed species. Atoms are colored as follows: O (red), C (grey), H (white), Pb (dark grey).

Table S13. Calculated free energies of reaction intermediates adsorbed on Pb(111).

Chemical species	**G (eV)**
FUR-CHO* (furfural*)	0.16
H*	0.82
FUR-CH_2O*	0.03
FUR-CH_2OH* (FA*)	-0.01
FUR-CHOH* (ketyl radical*)	0.75
FUR-CHO* + H* (IS for FUR-CH_2O* formation step)	1.00
FUR-CHO* + H* (IS for ketyl radical* formation step)	1.02
FUR-CHOH* + H* (IS for FA* formation step)	1.60
FUR-CHOH* + FUR-CHOH* (IS for HF* formation step)	1.51
$(FUR\text{-}CHOH)_2$ (HF*)	0.28

Table S14. Calculated activation free energy without potential dependent correction and U_0 (for electrochemical steps) of considered reaction steps on Pb(111).

Elementary step	**ΔG_{act} (eV)**	**U_0 (V_{RHE})**
FUR-CHOH* diffusion	0.25	-
FUR-CHOH* desorption	0.03	-
FUR-CHOH* → FUR-CH_2-OH*	0.24	-0.84
FUR-CHO* → FUR-CH-OH*	0.39	-0.86
FUR-CHO* → FUR-H_2C-O*	0.07	-0.84
FUR-CHOH* → $(FUR\text{-}CHOH)_2$*	0.48	-

Table S15. Calculated ΔG of considered reactions at -0.55 V_{RHE} on Pb(111) based on G of co-adsorbed species ($\Delta G_{coadsorbed} = G_{product} - G_{reactant1+reactant2}$) and G of species at infinite separation ($\Delta G_{infinite} = G_{product} - G_{reactant1} - G_{reactant2}$).

Elementary steps	$\Delta G_{coadsorbed}$ (eV)	$\Delta G_{infinite}$ (eV)
FUR-CHO* + H* → FUR-CH_2O*	-0.97	-0.95
FUR-CHO* + H* → FUR-CHOH*	-0.27	-0.23
FUR-CHOH* + H* → FUR-CH_2OH*	-1.61	-1.58
FUR-CHOH* + FUR-CHOH* → $(FUR\text{-}CHOH)_2$*	-1.32	-1.22

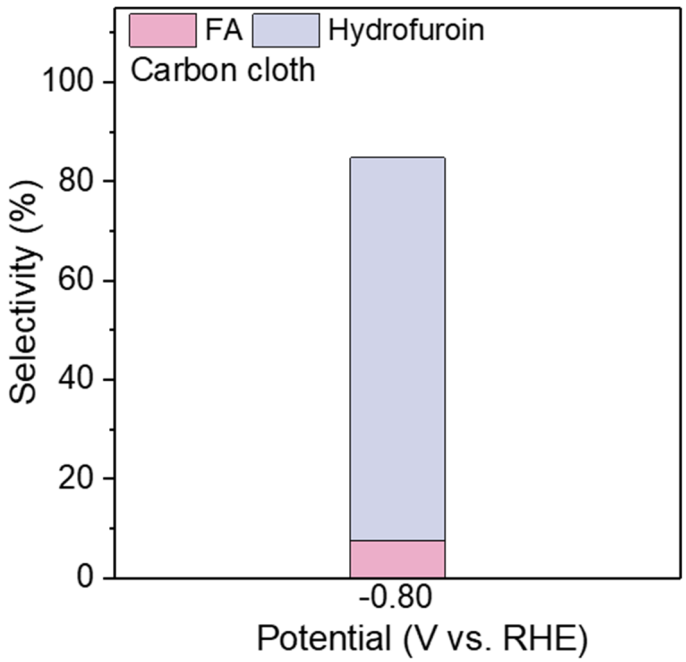

Figure S30. Product selectivity of 1-hour electrolysis of furfural on hydrophilic carbon cloth. The electrolysis was performed in pH = 7 buffer solution with 20 mM furfural.

References

1. Lee, C. H.; Kanan, M. W., Controlling H^+ vs CO_2 reduction selectivity on Pb electrodes. *ACS Catal.* **2015,** *5* (1), 465–469.
2. Choi, S. Y.; Jeong, S. K.; Kim, H. J.; Baek, I.-H.; Park, K. T., Electrochemical reduction of carbon dioxide to formate on tin–lead alloys. *ACS Sustain. Chem. Eng.* **2016,** *4* (3), 1311–1318.
3. Stoll S, Schweiger A. EasySpin: Simulating cw ESR spectra. Biol Magn Reson 2007;27:299–321. https://doi.org/10.1017/CBO9781107415324.004.
4. Chadderdon, X. H.; Chadderdon, D. J.; Matthiesen, J. E.; Qiu, Y.; Carraher, J. M.; Tessonnier, J.-P.; Li, W., Mechanisms of furfural reduction on metal electrodes: Distinguishing pathways for selective hydrogenation of bioderived oxygenates. *J. Am. Chem. Soc.* **2017,** *139* (40), 14120–14128.
5. Liu, H.; Lee, T.-H.; Chen, Y.; Cochran, E. W.; Li, W., Paired electrolysis of 5-(hydroxymethyl) furfural in flow cells with a high-performance oxide-derived silver cathode. *Green Chem.* **2021**.
6. Montgomery, H.; Thom, N.; Cockburn, A., Determination of dissolved oxygen by the Winkler method and the solubility of oxygen in pure water and sea water. *J. Appl. Chem.* **1964,** *14* (7), 280–296.
7. Kresse, G.; Hafner, J., Ab initio molecular dynamics for liquid metals. *Phys. Rev. B* **1993,** *47* (1), 558.
8. Kresse, G.; Hafner, J., Ab initio molecular-dynamics simulation of the liquid-metal–amorphous-semiconductor transition in germanium. *Phys. Rev. B* **1994,** *49* (20), 14251.
9. Kresse, G.; Furthmüller, J., Efficient iterative schemes for ab initio total-energy calculations using a plane-wave basis set. *Phys. Rev. B* **1996,** *54* (16), 11169.

10. Kresse, G.; Furthmüller, J., Efficiency of ab-initio total energy calculations for metals and semiconductors using a plane-wave basis set. *Comput. Mater. Sci.* **1996,** *6* (1), 15–50.
11. Perdew, J. P.; Chevary, J. A.; Vosko, S. H.; Jackson, K. A.; Pederson, M. R.; Singh, D. J.; Fiolhais, C., Atoms, molecules, solids, and surfaces: Applications of the generalized gradient approximation for exchange and correlation. *Phys. Rev. B* **1992,** *46* (11), 6671.
12. Perdew, J. P.; Chevary, J.; Vosko, S.; Jackson, K. A.; Pederson, M. R.; Singh, D.; Fiolhais, C., Erratum: Atoms, molecules, solids, and surfaces: Applications of the generalized gradient approximation for exchange and correlation. *Phys. Rev. B* **1993,** *48* (7), 4978.
13. Perdew, J. P.; Burke, K.; Ernzerhof, M., Generalized gradient approximation made simple. *Phys. Rev. Lett.* **1996,** *77* (18), 3865.
14. Grimme, S.; Ehrlich, S.; Goerigk, L., Effect of the damping function in dispersion corrected density functional theory. *J. Comput. Chem.* **2011,** *32* (7), 1456–1465.
15. Grimme, S.; Antony, J.; Ehrlich, S.; Krieg, H., A consistent and accurate ab initio parametrization of density functional dispersion correction (DFT-D) for the 94 elements H-Pu. *J. Chem. Phys.* **2010,** *132* (15), 154104.
16. Bengtsson, L., Dipole correction for surface supercell calculations. *Phys. Rev. B* **1999,** *59* (19), 12301.
17. Nørskov, J. K.; Rossmeisl, J.; Logadottir, A.; Lindqvist, L.; Kitchin, J. R.; Bligaard, T.; Jonsson, H., Origin of the overpotential for oxygen reduction at a fuel-cell cathode. *J. Phys. Chem. B* **2004,** *108* (46), 17886–17892.
18. Henkelman, G.; Jónsson, H., Improved tangent estimate in the nudged elastic band method for finding minimum energy paths and saddle points. *J. Chem. Phys.* **2000,** *113* (22), 9978–9985.
19. Henkelman, G.; Uberuaga, B. P.; Jónsson, H., A climbing image nudged elastic band method for finding saddle points and minimum energy paths. *J. Chem. Phys.* **2000,** *113* (22), 9901–9904.
20. Akhade, S. A.; Bernstein, N. J.; Esopi, M. R.; Regula, M. J.; Janik, M. J., A simple method to approximate electrode potential-dependent activation energies using density functional theory. *Catal.Today* **2017,** *288*, 63–73.
21. Rendon-Calle, A.; Low, Q. H.; Hong, S. H. L.; Builes, S.; Yeo, B. S.; Calle-Vallejo, F., How symmetry factors cause potential-and facet-dependent pathway shifts during CO_2 reduction to CH_4 on Cu electrodes. *Appl. Catal. B.* **2021,** *285*, 119776.
22. Monkhorst, H. J.; Pack, J. D., Special points for Brillouin-zone integrations. *Phys. Rev. B* **1976,** *13* (12), 5188.
23. Lu, Y.; Zhou, D.; Wang, T.; Yang, S. A.; Jiang, J., Topological properties of atomic lead film with honeycomb structure. *Sci. Rep.* **2016,** *6* (1), 1–7.
24. Frisch, M.; Trucks, G.; Schlegel, H.; Scuseria, G.; Robb, M.; Cheeseman, J.; Scalmani, G.; Barone, V.; Petersson, G.; Nakatsuji, H., Gaussian 09, Revision A.02. Gaussian, Inc. Wallingford, CT: **2016.**
25. McLean, A.; Chandler, G., Contracted Gaussian basis sets for molecular calculations. I. Second row atoms, Z= 11–18. *J. Chem. Phys.* **1980,** *72* (10), 5639–5648.
26. Raghavachari, K.; Trucks, G. W., Highly correlated systems. Excitation energies of first row transition metals Sc–Cu. *J. Chem. Phys.* **1989,** *91* (2), 1062–1065.
27. Marenich, A. V.; Cramer, C. J.; Truhlar, D. G., Universal solvation model based on solute electron density and on a continuum model of the solvent defined by the bulk dielectric constant and atomic surface tensions. *J. Phys. Chem. B* **2009,** *113* (18), 6378–6396.
28. Sanyal, U.; Yuk, S. F.; Koh, K.; Lee, M. S.; Stoerzinger, K.; Zhang, D.; Meyer, L. C.; Lopez-Ruiz, J. A.; Karkamkar, A.; Holladay, J. D., Hydrogen bonding enhances the electrochemical hydrogenation of benzaldehyde in the aqueous phase. *Angew. Chem.* **2021,** *133* (1), 294–300.
29. Singh, N.; Sanyal, U.; Fulton, J. L.; Gutiérrez, O. Y.; Lercher, J. A.; Campbell, C. T., Quantifying adsorption of organic molecules on platinum in aqueous phase by hydrogen site blocking and in situ X-ray absorption spectroscopy. *ACS Catal.* **2019,** *9* (8), 6869–6881.
30. Akinola, J.; Barth, I.; Goldsmith, B. R.; Singh, N., Adsorption energies of oxygenated aromatics and organics on rhodium and platinum in aqueous phase. *ACS Catal.* **2020,** *10* (9), 4929–4941.

31. Anibal, J.; Xu, B., Electroreductive C–C Coupling of Furfural and Benzaldehyde on Cu and Pb Surfaces. *ACS Catal.* **2020,** *10* (19), 11643–11653.
32. Cantu, D. C.; Padmaperuma, A. B.; Nguyen, M.-T.; Akhade, S. A.; Yoon, Y.; Wang, Y.-G.; Lee, M.-S.; Glezakou, V.-A.; Rousseau, R.; Lilga, M. A., A combined experimental and theoretical study on the activity and selectivity of the electrocatalytic hydrogenation of aldehydes. *ACS Catal.* **2018,** *8* (8), 7645–7658.
33. Sanyal, U.; Yuk, S. F.; Koh, K.; Lee, M.-S.; Stoerzinger, K.; Zhang, D.; Meyer, L. C.; Lopez-Ruiz, J. A.; Karkamkar, A.; Holladay, J. D., Hydrogen bonding enhances the electrochemical hydrogenation of benzaldehyde in the aqueous phase. *Angew. Chem.* **2021***, 133* (1), 294–300.
34. Singh, N.; Sanyal, U.; Ruehl, G.; Stoerzinger, K. A.; Gutiérrez, O. Y.; Camaioni, D. M.; Fulton, J. L.; Lercher, J. A.; Campbell, C. T., Aqueous phase catalytic and electrocatalytic hydrogenation of phenol and benzaldehyde over platinum group metals. *J. Catal.* **2020,** *382*, 372–384.
35. Andrews, E.; Lopez-Ruiz, J. A.; Egbert, J. D.; Koh, K.; Sanyal, U.; Song, M.; Li, D.; Karkamkar, A. J.; Derewinski, M. A.; Holladay, J., Performance of base and noble metals for electrocatalytic hydrogenation of bio-oil-derived oxygenated compounds. *ACS Sustain. Chem. Eng.* **2020,** *8* (11), 4407–4418.
36. Lopez-Ruiz, J. A.; Sanyal, U.; Egbert, J.; Gutiérrez, O. Y.; Holladay, J., Kinetic investigation of the sustainable electrocatalytic hydrogenation of benzaldehyde on Pd/C: effect of electrolyte composition and half-cell potentials. *ACS Sustain. Chem. Eng.* **2018,** *6* (12), 16073–16085.
37. Sun, S.; Zhang, G.; Geng, D.; Chen, Y.; Li, R.; Cai, M.; Sun, X., A highly durable platinum nanocatalyst for proton exchange membrane fuel cells: multiarmed starlike nanowire single crystal. *Angew. Chem.* **2011,** *123* (2), 442–446.
38. Banerjee, S.; Han, X.; Thoi, V. S., Modulating the electrode–electrolyte interface with cationic surfactants in carbon dioxide reduction. *ACS Catal.* **2019,** *9* (6), 5631–5637.
39. Banerjee, S.; Zhang, Z.-Q.; Hall, A. S.; Thoi, V. S., Surfactant Perturbation of Cation Interactions at the Electrode–Electrolyte Interface in Carbon Dioxide Reduction. *ACS Catal.* **2020,** *10* (17), 9907–9914.
40. Aikens, D., Electrochemical methods, fundamentals and applications. ACS Publications: 1983, 534–577.
41. Wesley, T. S.; Román-Leshkov, Y.; Surendranath, Y., Spontaneous Electric Fields Play a Key Role in Thermochemical Catalysis at Metal− Liquid Interfaces. *ACS Cent. Sci.* **2021,** *7* (6), 1045–1055.
42. Ryu, J.; Surendranath, Y., Tracking electrical fields at the Pt/H2O interface during hydrogen catalysis. *J. Am. Chem. Soc.* **2019,** *141* (39), 15524–15531.
43. Singh, M. R.; Kwon, Y.; Lum, Y.; Ager III, J. W.; Bell, A. T., Hydrolysis of electrolyte cations enhances the electrochemical reduction of CO2 over Ag and Cu. *J. Am. Chem. Soc.* **2016,** *138* (39), 13006–13012.
44. Li, J.; Li, X.; Gunathunge, C. M.; Waegele, M. M., Hydrogen bonding steers the product selectivity of electrocatalytic CO reduction. *Proc. Natl. Acad. Sci.* **2019,** *116* (19), 9220–9229.